



From an accretionary margin to a sediment-rich collision: Spatiotemporal evolution of the magmatism during the closure of the Mongol-Okhotsk Ocean



Susana Henriquez^{a,b,*}, Ochir Gerel^c, Sarah Lambart^a, Cari L. Johnson^a, Laura E. Webb^d, Peter C. Lippert^a

^a University of Utah, Geology and Geophysics, Salt Lake City, UT, United States

^b California State University San Bernardino, Geological Sciences, San Bernardino, CA, United States

^c Mongolian University of Science and Technology, Geoscience Center, Ulaanbaatar, Mongolia

^d University of Vermont, Geography & Geosciences, Burlington, VT, United States

ARTICLE INFO

Article history:

Received 27 October 2023

Revised 30 June 2024

Accepted 1 July 2024

Available online 3 August 2024

Handling editor: Yongjiang Liu

Keywords:

Mongol-Okhotsk Ocean

Subduction-related magmatism

Geochemistry

Sediment melts

Crustal assimilation

ABSTRACT

The closure of the Mongol-Okhotsk Ocean (MOO) marks the final suturing of the Central Asian Orogenic Belt, one of the largest accretionary orogens on Earth and a region that is considered an archetype for crustal growth during the Phanerozoic. Abundant Permian to Triassic magmatism in Mongolia extended into the Jurassic on the eastern side of the Mongol-Okhotsk Belt (MOB), the orogenic belt produced by the closure of the MOO. Magmatic belts formed north and south of the suture along the MOB provide insight into the dynamics of the subduction system and the magmatic, crustal, and mantle processes pre-, syn- and post- collision within this accretionary margin. One of the main questions regarding the magmatism in the region is: Was the magmatism formed during active subduction or during the collision and closure of the basin? Here we compile geochemical data (major and trace elements, and isotopes) from the Permian to Jurassic magmatic rocks in the MOB and analyze their spatiotemporal characteristics. Our goal is to assess how magmatism changed in time and space during the closure of the Mongol-Okhotsk Ocean and how those changes relate to first-order tectono-magmatic processes right before or during the collisional event that closed the basin. Our results show a general enrichment in fluid mobile elements, LILE, and LREE and depletion in HFSE, and HREE in mafic and felsic rocks, which indicates a mantle metasomatized by subduction-related fluids regardless of crustal contamination. Our analysis supports higher enrichment in sediment melts, especially along its western and older extent, and the assimilation of juvenile crustal components without producing abundant S-type peraluminous magmatism which indicates mantle and crustal contributions. Thus, we conclude that magmatism formed above a sediment-rich retreating margin was able to recycle and stabilize young and compositionally evolved crustal material in the Central Asian Orogenic Belt.

© 2024 Published by Elsevier B.V. on behalf of International Association for Gondwana Research.

1. Introduction

The Late Paleozoic–Early Mesozoic Mongol-Okhotsk Ocean extended between the Siberian craton and Amur–North China block (e.g., Zonenshain et al., 1990; Sengör and Natal'in, 1994; Zorin, 1999; Xiao et al., 2018). Today, the Mongol-Okhotsk Belt (MOB) is an orogenic belt that extends over 3000 km from the Khangay mountains in central Mongolia to the Sea of Okhotsk and includes an island arc, accretionary complexes, magmatic belts, and the Mongol-Okhotsk suture zone (Fig. 1a; Wang et al., 2017; Zonenshain et al., 1990). This orogenic belt formed by the

closure of the Mongol-Okhotsk Ocean, the youngest accretionary event within the Central Asian Orogenic Belt (CAOB) (e.g., Xiao et al., 2018); however, the timing, kinematics, and geodynamic processes that led to this closure remain unresolved.

Permian to Triassic magmatism is abundant in the MOB. The magmatic belts are oriented E-NE and form provinces north and south of the suture, which is interpreted to indicate double-sided or folded subduction during the closure of the ocean (e.g., Tomurtogoo et al., 2005; Tang et al., 2016; Li et al., 2013; Sheldrick et al., 2020; Wang et al., 2021a). Magmatic provinces along the MOB are generally characterized by an enrichment in subduction components (e.g., Gerel and Munkhtsengel, 2004; Berzina et al., 2009; Donskaya et al., 2012, 2013; Li et al., 2013; Tang et al., 2014, 2016; Sheldrick et al., 2020; Ganbat et al., 2021,

* Corresponding author.

E-mail address: susana.henriquez@csusb.edu (S. Henriquez).

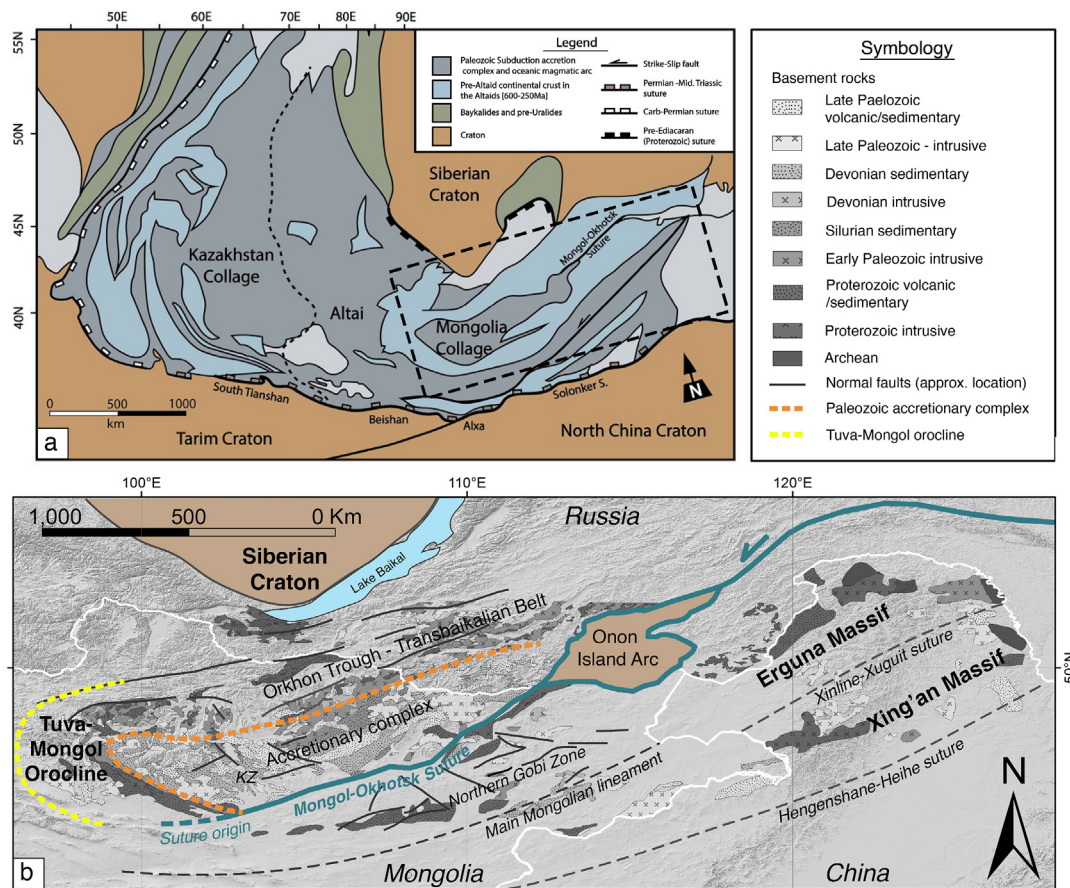


Figure 1. a) Tectonic map. b) Tectonic elements of the Mongol-Okhotsk Belt. Modified from Yarmolyuk et al. (2013), Han et al. (2015), Tang et al. (2016), and Li et al. (2022).

2022); however, crustal contamination by rocks formed above a long-lived subduction zone, or magmatism in a region previously affected by subduction, such as the one in the Mongol-Okhotsk belt, could also have produced an enrichment in subduction-related elements (Yarmolyuk et al., 2002, 2013; Tsygankov et al., 2017).

The lack of precise independent constraints for the timing of closure in the western side of the Mongol-Okhotsk Belt complicates understanding the geodynamic configuration of the magmatism. Igneous geochemistry, however, can record mantle and crustal processes, and magmatic rocks provide information about the tectono-magmatic conditions along the paleo-margin and during the collision. These data have implications for how the magmatic signatures relate to continental assembly through collisional processes.

While the presence of a mantle plume after the closure of the MOO has been proposed as a driver of magmatism in the region (e.g., Yarmolyuk et al., 2002; Tsygankov et al., 2017), the geochemical data compiled in this study favor the role of an active (or recently active) subduction system during the closure (as detailed in the subsequent sections). Previous compilations about the Permian to Jurassic magmatism related to the Mongol-Okhotsk Belt (e.g., Donskaya et al., 2013; Li et al., 2013; Wang et al., 2021a) have recognized the role of subduction components and juvenile and crustal components in the magmatism, the eastward migration of the magmatism and generally consider that a mantle plume could have interacted with the subduction in the western end of the MOB. However, the presence of subduction fluids despite crustal contributions, and the spatiotemporal changes in crustal and hydrous melt contributions pre-, syn-, and post-collision, especially near the core of the orocline, remain undetermined. Hence, we test the scenario in which magmatism within the MOB is

explained by subduction-related magmatism and hypothesize that a scissor-like closure influenced the magmatic signature through higher assimilation of crustal components near the core of the orocline in the western region of the MOB. We focus on two questions: (1) Is the signature of mantle enrichment by subduction related fluids preserved regardless of crustal contamination? (2) Is there a difference in the geochemical signatures associated with mantle and crustal processes along and across the suture? To address these two questions, we compiled geochemical data from igneous rocks formed in the Permian to Jurassic igneous belts. The database comprises major and trace elements, whole rock Sm-Nd isotopic data, and zircon Lu-Hf isotopic data. We review these data in time and space with the goal of identifying petrogenetic, mantle, and crustal processes. Our results show that a mantle source was enriched in subduction-related components, which indicates active or recently active subduction near the western extent of the suture until the Late Triassic. Moreover, we show that geochemical data reveal that assimilation of crustal components and sediment melts were higher in the internal magmatic belts near the western and presumably older segment of the suture during the Permian and Triassic. This reflects the effect of a sediment-rich retreating margin, high temperature conditions, and magmatic processes that led to the preservation and stabilization of the crust during the final stages of suturing.

2. Tectonic Setting

2.1. The Central Asian Orogenic Belt and the Mongolia Collage System

The Central Asian Orogenic Belt (CAOB) is located between the Siberian Craton and the Tarim and North China Cratons and

extends from the Urals to the Sea of Okhotsk (Fig. 1; e.g., Xiao et al., 2003; Windley et al., 2007). The CAOB was formed by the accretion of island arcs, seamounts, accretionary wedges, and microcontinents between the latest Mesoproterozoic (ca. 1 Ga) and early Mesozoic (Khain, 2003; Xiao et al., 2003, 2004; Zonenshain et al., 1990), which led to the closure of the Paleo-Asian Ocean (e.g., Şengör et al., 1993; Windley et al., 2007; Kurihara et al., 2009; Wilhem et al., 2012; Xiao et al., 2015). These accretionary processes were accompanied by the widespread production of large volumes of granitoid rocks typically with juvenile isotopic signatures along the CAOB (e.g., Wang et al., 2017) which are consistent with the assimilation of crustal host rocks (e.g., Kozlovsky et al., 2023).

The CAOB can be divided into three collage systems: Kazakhstan, Tarim-North China, and Mongolia collage systems (Xiao et al., 2015). The Mongolia collage system is the youngest collage and includes several zones (Lake, Gobi-Altai, Trans-Altai, and South Gobi) which, by the latest Carboniferous, tailed the southern end of the Tuva-Mongol and Zavkhan-Baydrag amalgamated continental blocks (Xiao et al., 2015). During the late Permian to Early Triassic, the clockwise rotation of these blocks led to the closure of the Solonker ocean (Paleo-Asian Ocean) and the formation of the Solonker suture between the Mongolia collage system to the north and the North China Craton to the south (Xiao et al., 2015 and references therein). The Solonker suture extends toward NE China where the Mongolia collage system includes the Erguna, Xing'an, and Songliao blocks (e.g., Han et al., 2015) which are separated by the early Paleozoic Xinline-Xuguit suture and the late Paleozoic Hengshane-Heihe suture, respectively (e.g., Miao et al., 2008; Zhou and Wilde, 2013).

2.2. Formation and collapse of the Mongol-Okhotsk Belt (MOB)

The mechanisms that led to the closure of the Mongol-Okhotsk Ocean (MOO) are still debated. Two fundamental modes of closure have been proposed: a scissor-like closure of an oceanic gateway (e.g., Parfenov et al., 2010; Fritzell et al., 2016; Wu et al., 2017) or an oroclinal closure (e.g., Şengör et al., 1993; Edel et al., 2014; Van der Voo et al., 2015; Li et al., 2022) wherein the entire lithosphere buckled (Johnston et al., 2013; Kilian et al., 2016). Although both models explain the eastward closure of the MOO, the main difference between these two models lies in the fact that the closure of a gateway requires that the suture extends west of the Khangay dome in central Mongolia (e.g., Parfenov et al., 2010). In contrast, oroclinal closure proposes that the Tuva-Mongol orocline in central Mongolia and the western end of Mongol-Okhotsk suture zone would have accommodated significant horizontal rotations (e.g., Xiao et al., 2010; Van der Voo et al., 2015).

The Permian to Triassic rift belts north, west, and south of the suture must also be considered in any tectono-magmatic evolution of this region. Slab roll-back, a process that appears to have played an important role during the closure of the CAOB (Xiao et al., 2018; Wang et al., 2021a), is often related to upper plate extension (e.g., Schellart, 2004; Nakakuki and Mura, 2013), and could have formed back-arc basins, both around the orocline and subparallel to the suture zone during the closure of the MOO. Similarly, the closure of a gateway could also have been accompanied by slab roll-back and upper plate extension.

The collision and final suturing of the MOO formed the Mongol-Okhotsk Belt (Mongolia-Okhotsk collisional belt and related magmatism; Zorin 1999), a collisional belt that includes folded middle Paleozoic to early Mesozoic sequences such as a Paleozoic accretionary complex (Kelty et al., 2008; Kurihara et al., 2009), Carboniferous ophiolites (Tomurtogoo et al., 2005), tectonic mélanges (Sorokin et al., 2020), and Triassic to Jurassic marine sedimentary

rocks (Ehiro et al., 2006; Sorokin et al., 2020; Arzhannikova et al., 2022), the Onon island arc (Zorin, 1999), Triassic strike-slip fault systems (e.g., the Muron fault along the Mongol-Okhotsk suture zone; Tomurtogoo et al., 2005), and abundant Permian to Triassic magmatism (e.g., Donskaya et al., 2013; Antipin et al., 2019; Tang et al., 2016) on both sides of the suture. Additionally, a series of regional high-angle structures of undetermined time history (e.g., Mongolian Lineament, and the Kharkhorin, Bayangol, Yeroogol, and South Khentei faults; e.g., Badarch et al., 2002; Onon and Tsukada, 2017) control the distribution and structural orientation of terranes within the MOB. Permian to Jurassic magmatic belts are aligned within the MOB, found within and north of the Onon island arc (Figure 2; e.g., Zorin 1999; Tang et al., 2016), and along the edges of the MOB. On the northern side of the suture, the Khangay and Khentey batholiths are exposed in Mongolia and southern Russia (e.g., Yarmolyuk et al., 2002; Orolmaa et al., 2008; Antipin et al., 2016). South of the suture, the Middle Gobi Volcanoplutonic Belt (e.g., Gerel et al., 2017) in Mongolia extends into NE China as magmatism in the Erguna Massif (e.g., Tang et al., 2016). Magmatism along the edges of the MOB comprises volcanoplutonic belts controlled by the presence of rift basins north (Mongolian Transbaikalian belt, e.g., Vorontsov et al., 2007; Berzina et al., 2009; Donskaya et al., 2013) and south of the suture (Middle Gobi Volcanoplutonic Belt and magmatism in the Xing'an Massif; e.g., Zhu et al., 2016; Li et al., 2016). Magmatism is typically enriched in subduction-related fluids (e.g., Donskaya et al., 2013; Tang et al., 2016; Liu et al., 2018). This geochemical signature, however, could have been inherited from material assimilated during magma ascent (e.g., Kuzmin et al., 2011; Yarmolyuk et al., 2013; Tsygankov et al., 2017).

Several constraints for the timing of suturing of the Mongol-Okhotsk Ocean exist. In central Mongolia, the Adaatsag ophiolite that includes a leucogabbro pegmatite dike dated at 325.4 ± 1.1 Ma ($^{207}\text{Pb}/^{206}\text{Pb}$ evaporation age) provides one of the few direct constraints for presence of the Mongol-Okhotsk Ocean (Tomurtogoo et al., 2005). Early Triassic marine sedimentary rocks evidence the presence of the Mongol-Okhotsk Ocean basin in eastern Mongolia (Ehiro, 2006). In southern Russia (eastern MOB), the absence of U-Pb ages younger than ca. 171 Ma in detrital zircons from the metasedimentary rocks formed in tectonic mélanges within the Mongol-Okhotsk Belt is considered a signal the final closure of this basin (Sorokin et al., 2020). Shallow marine deposits in the Mohe-Upper Amur Basin (southern side of the suture), sourced from the south ca. 155–145 Ma, were covered by intermontane deposits sourced from the north, indicating the transition from an extensional (pre ca. 155–145 Ma) to a contractional setting (Guo et al., 2017). Farther to the east, the development of a peripheral foreland basin that formed between 165–155 Ma also marks the timing of closure in the eastern side of the MOO (Arzhannikova et al., 2022).

During the Jurassic and Cretaceous, the MOB collapsed and formed a series of extensional basins (e.g., Meng et al., 2003). Extensional processes that followed the collisional event extended from southern Russia, through Mongolia and China, and include several NE to ENE oriented extensional basins and metamorphic core complexes (e.g., Meng et al., 2003; Daoudene et al., 2009; Dash et al., 2015; Ritts et al., 2010; Jolivet et al., 2017).

3. Methods

We compiled major and trace element compositions and isotopic ratios of Permian to Jurassic igneous samples along the Mongol-Okhotsk Belt from central Mongolia to NE China from the published literature and geochemical databases.

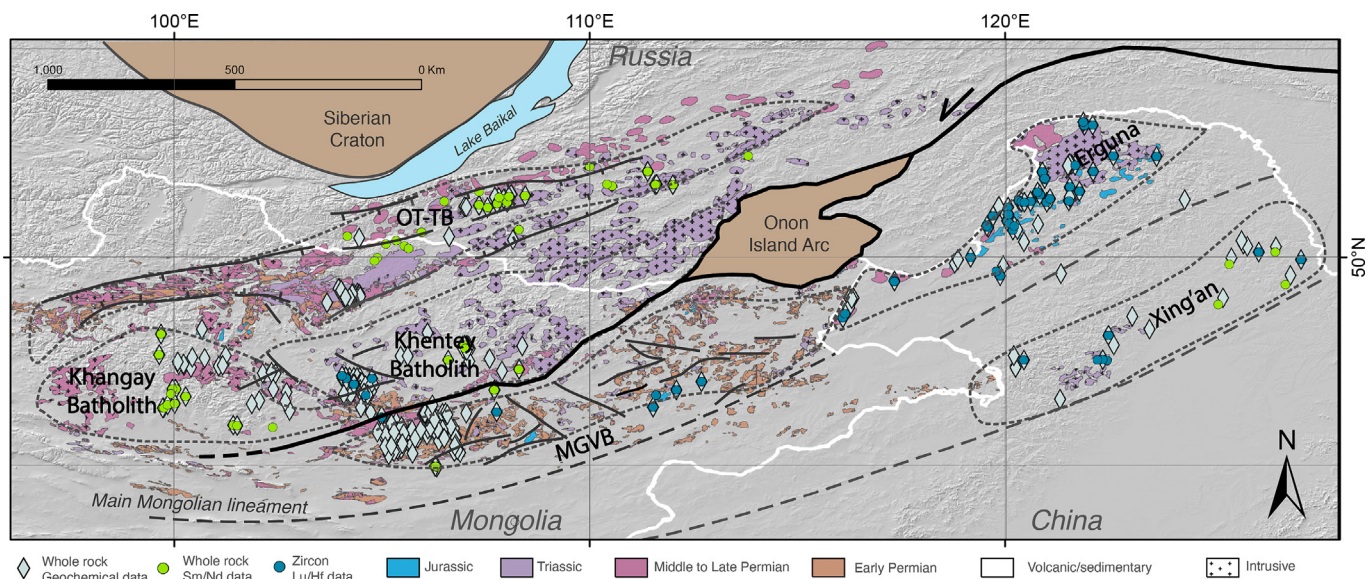


Figure 2. Geologic map showing the distribution of the magmatic provinces and geochemical (major and trace) and isotopic data. OT-TB: Orkhon Trough-Transbaikalian Belt. MGVB: Middle Gobi Volcanoplutonic Belt.

3.1. Geochemical Database of Igneous Rocks

The element database consists of major and trace elements, including rare earth elements (REE) for 829 individual samples from 39 studies. Metadata includes age, location, method, and laboratory information. The isotopic database incorporates 896 samples, 622 samples with zircon Lu-Hf, 180 samples with Rb-Sr, and 168 samples with Sm-Nd isotopic data. The isotope database includes age and location information. Data were extracted from published studies that summarized previous data compilations (Wu et al., 2011; Liu et al., 2018; Wang et al., 2021a). Data and details about the database are available in two online repositories (<https://doi.org/10.7278/S50d-0phb-z0x0> and <http://doi.org/10.7278/S50d-fraf-ds5g>). The criterion for data quality is explained in the description of each online repository. To reduce uncertainties related to alteration, samples producing high total volatile content (LOI > 5 wt%) were removed. Additionally, we used the alteration box (Fig. S1; Large, 2001) to identify and filter out samples that follow hydrothermal alteration trends.

3.2. Spatial Distribution of Geochemical Data

The available geochemical data covers magmatic provinces north and south of the suture (Fig. 2); however, the spatial distribution is heterogeneous. Areas such as the western side of the Orkhon Trough-Transbaikalian Belt and the eastern side of the Khentey Batholith are not represented in this compilation. Data east of the Middle Gobi Volcanoplutonic Belt and west of the Erguna and Xing'an magmatic provinces are sparse. This work relies on observations made in areas with relatively high data density (Fig. 2). Nonetheless, future work and data, especially in under-sampled regions, will further our understanding of the magmatic processes during the closure of the MOO. This compilation underscores where geochemical data are most needed in time and space within the MOB.

4. Results: Magmatism in the Mongol-Okhotsk Belt

Magmatism related to the Mongol-Okhotsk Ocean started in Cambrian and ended in Jurassic times (e.g., Donskaya et al., 2013; Wang et al., 2021a). Igneous rocks limited to the Mongol-

Okhotsk Belt are mainly Permian to Jurassic in age and were formed during the later stages of the Mongol-Okhotsk basin, during its closure and in its post-collisional setting (e.g., Gerel and Munkhtsengel, 2004; Orolmaa et al., 2008; Donskaya et al., 2013; Zhu et al., 2016). Five main magmatic provinces were formed during this time: the Orkhon Trough-Transbaikalian Belt, the Khangay Batholith, the Khentey Batholith, the Middle Gobi Volcanoplutonic Belt, and the Erguna-Xing'an magmatic province (Fig. 2). A description of each magmatic province, their major element characteristics, and their trace element compositions are provided below. Special attention was paid to subduction-like signatures which provide insight into the presence or absence of a mantle metasomatized by subduction related fluids and possible spatiotemporal changes in the magma source or crustal additions.

4.1. Magmatic Provinces and Their Major Element Geochemical Composition

4.1.1. Khangay and Khentey Batholiths

The Khangay Batholith is a Middle Permian to Middle Triassic (270–240 Ma) igneous province located in the western end of the Mongol Okhotsk Belt (Fig. 2; e.g., Yarmolyuk et al., 2002, 2008; Jahn et al., 2004; Orolmaa et al., 2008). It was emplaced in a Devonian to Carboniferous accretionary complex (Kelty et al., 2008; Kurihara et al., 2009). Khangay Batholith is composed mainly of granites and granodiorites with subordinate quartz diorite, tonalite and alkali granite. The Khentey Batholith is a Late Triassic to Early Jurassic (230–180 Ma) igneous province located in central Mongolia (Fig. 2). Its western end overlaps part of the Khangay Batholith and was also emplaced in the Devonian to Carboniferous accretionary complex (Kelty et al., 2008; Kurihara et al., 2009). Compositionally, this batholith consists of granodiorites to leucogranites with subordinate gabbro and diorites (Kovalenko et al., 1984; Yarmolyuk et al., 2002). Magmatism ended with small leucogranite dikes and stocks and lithium-fluorine granites emplaced in the southwestern margin of the batholith (Fig. 2; Antipin et al., 2016; Yarmolyuk et al., 2002). In the western end of the Khentey Batholith, magmatism is associated with coeval volcanic rocks that rest on an erosional unconformity over granitoids from the Khangay Batholith (Yarmolyuk et al., 2013).

Granitoids from the Khangay Batholith (Jahn et al., 2004; Orolmaa et al., 2008) are subalkaline, high-K calc-alkaline to shoshonitic (Figs. 3a; Orolmaa et al., 2008), metaluminous (Figs. 3c; Orolmaa et al., 2008), magnesian (Fig. 3e), and I-type (Figs. 3e,g; Jahn et al., 2004). In comparison, the plutonic rocks from the Khentey Batholith (Jahn et al., 2004, 2009; Antipin et al., 2016, 2019) are subalkaline to alkaline (Fig. 3a), high-K calc-alkaline to shoshonitic (Fig. 3c), metaluminous (Fig. 3e), magnesian and ferroan (Fig. 3e; e.g., Donskaya et al., 2013), and I-, S-types (Fig. 3g) and A2-type. Samples from the Khangay and Khentey Batholiths present similar trace element patterns (Fig. S2) with the most enriched samples – defined here as samples with Sr concentration normalized to the primitive mantle, $Sr_N > 10$ – showing positive anomalies in Pb, U and Th and relatively fractionated heavy REE (HREE), while less enriched samples ($Sr_N < 10$) show strong negative anomalies in Ba, Sr, and Eu and relatively flat MREE to HREE trends. Some depleted samples from the Khentey Batholith however show positive anomalies in Pr and Sm, not observed in samples from the Khangay Batholith.

4.1.2. Orkhon Trough - Transbaikalian Belt

The Orkhon Trough-Transbaikalian Belt (OT-TB) extends along northern Mongolia and southern Siberia (Figs. 1b and 2; e.g., Gerel and Munkhtsengel, 2004; Vorontsov et al., 2007; Yarmolyuk et al., 2013; Tsygankov et al., 2017). It was emplaced in a heterogeneous crust formed by Proterozoic oceanic terranes, Proterozoic to Paleozoic metamorphic and volcanic rocks, and Paleozoic shallow marine clastic sedimentary and carbonate rocks (e.g., Badarch et al., 2002; Tsygankov et al., 2017). The western part of the OT-TB, north of the Khangay Batholith (Fig. 2), consists of mainly Permian basalts and basalt-trachyte-pantellerite volcanics and alkaline granites, syenites, and gabbro-monzonites (North Mongolian Rift Zone; Yarmolyuk et al., 2013). The central part of the OT-TB, north of Khentey Batholith in northern Mongolia, consists of Permian volcanic rocks (Khanui Group) with a bimodal chemical composition (Orkhon Trough; Gerel and Munkhtsengel, 2004; Munkhtsengel et al., 2007), a Permian sequence of intermediate lavas, tuff breccia and conglomerate (Mogod Formation according to Tsukada et al., 2022), Permian to Triassic intrusive complexes (Selenge and Erdenet plutonic complexes; e.g., Gerel and Munkhtsengel, 2004; Munkhtsengel et al., 2007), and Middle to Upper Triassic and Jurassic volcanic rocks with basaltic, and trachybasaltic to trachydacitic compositions (Mogod Formation according to Munkhtsengel et al., 2007). We note that Tsukada et al. (2022) suggested a revision of the igneous ages in this area after obtaining Permian ages for two igneous samples from the Mogod Formation, a unit previously considered Middle to Upper Triassic and Jurassic (Munkhtsengel et al., 2007). The authors argue that the previous K-Ar ages might be dating alteration. However, their lithologic description for the Mogod Formation differs from the one by Munkhtsengel et al. (2007) (see above). Other studies in the central part of the OT-TB have provided age constraints for magmatism during the Late Triassic (e.g., Berzina et al., 2009; Donskaya et al., 2012). Thus, we consider that Permian and Triassic volcanism took place in the central part of the OT-TB, and agree that the age and distribution of the Permo-Triassic volcanism need to be revised. The eastern part of the OT-TB, which extends into Russia, comprises Upper Triassic–Lower Jurassic compositionally bimodal volcanic rocks usually confined to grabens and alkaline and subalkaline intrusions (Western Transbaikalian; e.g., Yarmolyuk et al., 2002; Vorontsov et al., 2007). Late Triassic peralkaline and alkali-feldspar syenites and granites are commonly associated with the bimodal volcanism (Jahn et al., 2009).

Major element geochemical composition of magmatic rocks from the OT-TB indicates subalkaline and alkaline (bimodal) compositions up to the Early Triassic and alkaline by the Jurassic

(Fig. 3b; Gerel and Munkhtsengel, 2004; Vorontsov et al., 2007; Berzina et al., 2009; Reichow et al., 2010; Donskaya et al., 2012). These igneous rocks exhibit medium, high-K calc-alkaline and shoshonitic signatures (Fig. 3b,d). The rocks are metaluminous and both magnesian and ferroan (Figs. 3f). Additionally, they also include I-type (Fig. 3f) and A2-type granites (Donskaya et al., 2013). The enriched samples ($Sr_N > 10$), that corresponds to Permian-Triassic rocks with mafic to felsic compositions (Fig. S2), show positive anomalies in Ho and Tm not observed in the Khangay and Khentey Batholiths. These samples also lack of a strong Pb positive anomaly. The depleted samples ($Sr_N < 10$), composed of exclusively high silica samples and mostly Late Triassic in age, are enriched in light REE (LREE) compared to HREE and have flat MREE-HREE patterns (Fig. S2).

4.1.3. Middle Gobi Volcanoplutonic Belt

The Middle Gobi Volcanoplutonic Belt (MGVB), as defined by Badarch et al. (2002), is oriented NNE between the suture zone and the Main Mongolian Lineament (MML). It extends for about 1000 km with a width of 100 km approximately and includes Permian and Triassic plutonic and volcanic rocks structurally controlled by an extensional fault system (e.g., Yarmolyuk et al., 2013). It was emplaced in a heterogeneous crust that includes Proterozoic plutonic, metamorphic, ophiolitic, volcanic, and volcanoclastic rocks and Paleozoic intrusive, volcanic, volcanoclastic, and shallow marine rocks (Badarch et al., 2002). Middle to late Permian magmatism includes granites, quartz syenites, and monzonites (Gerel et al., 2017; Zhao et al., 2017). The subsequent Middle Triassic to Early Jurassic igneous record includes intrusive and volcanic rocks (Machowiak and Stawikowski, 2012; Zhu et al., 2016; Sheldrick et al., 2020). In the western side, the MGVB consists of syenites, granites, leucogranites, and granitoids (Yarmolyuk et al., 2002; Gerel et al., 2017; Machowiak and Stawikowski, 2012), and basaltic dikes, basalts, basalt-comendite volcanics, basalt-andesites, trachytes, and rhyolites (Yarmolyuk et al., 2002; Zhu et al., 2016).

Igneous rocks from the Middle Gobi Volcanoplutonic Belt are subalkaline, mainly felsic with subordinate intermediate and mafic compositions up to the Early Triassic that vary to bimodal by the Middle Triassic (Figs. 3a,b; e.g., Zhu et al., 2016; Gerel et al., 2017; Zhao et al., 2017; Ganbat et al., 2022). Felsic rocks have high-K calc-alkaline to shoshonitic signatures while mafic rocks exhibit medium to high-K calc-alkaline signatures (Figs. 3c,d). Permian to Early Triassic rocks are magnesian, I-type, and both metaluminous and peraluminous (Fig. 3e,f,g,h). By the Late Triassic, magmatism is mainly ferroan and secondarily magnesian, mainly metaluminous, and both I-type and A2-type with subordinate S-type (Fig. 3e,f,g,h; Machowiak and Stawikowski, 2012; Zhu et al., 2016; Zhao et al., 2017). Trace elements are only available for Permian and Late Triassic samples. All samples are moderately enriched in LREE compared to MREE and HREE and show relatively flat trends for MREE and HREE (Fig. S2). Permian magmatism is generally less enriched in trace elements than Late Triassic magmatism.

4.1.4. Erguna and Xing'an Magmatic Provinces

The Erguna and Xing'an massifs in NE China are intruded by a series of Early Mesozoic igneous rocks during Middle Permian to Late Jurassic times (e.g., Tang et al., 2014, 2016; Li et al., 2016, 2017; Liu et al., 2018). We refer to these igneous rocks as the Erguna and Xing'an magmatic provinces. The basement of this province is composed of Neoproterozoic to Paleozoic granitoids and Paleoproterozoic metamorphic rocks (e.g., Wu et al., 2011; Li et al., 2017). Plutonic and volcanic rocks crop out in NE oriented belts (Fig. 2). The northern belt is closer to the suture and includes Triassic and Early Jurassic intrusives dominated by felsic composi-

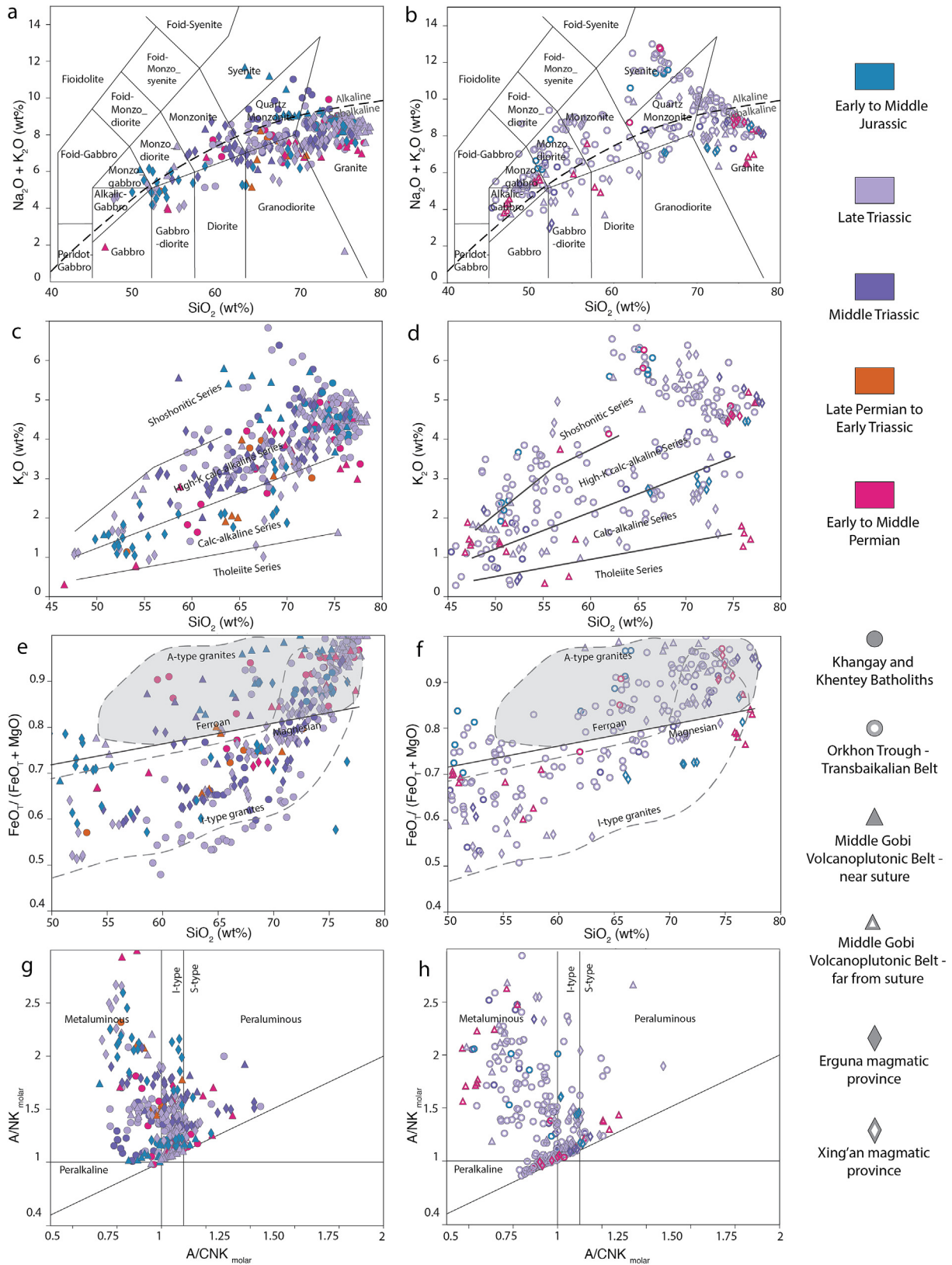


Figure 3. Geochemical plots based on major oxides. Plots in the left column show data for magmatic provinces near the suture (filled symbols). Plots in the right column show data for magmatic provinces away from the suture (empty symbols). From top to bottom, the plots are: a-b) Total alkali vs SiO_2 (TAS; Middlemost, 1994), c-d) K_2O vs. SiO_2 (Peccerillo and Taylor, 1976), e-f) $\text{FeO}_T/(\text{FeO}_T + \text{MgO})$ vs. SiO_2 (Frost et al., 2001), and g-h) $\text{Al}_2\text{O}_3/(\text{Na}_2\text{O} + \text{K}_2\text{O})$ vs. $\text{Al}_2\text{O}_3/(\text{Na}_2\text{O} + \text{K}_2\text{O} + \text{CaO})$ (Maniar and Piccoli, 1989) discrimination diagrams.

tions and only subordinately mafic rocks (Liu et al., 2018). Middle Triassic intrusive rocks consist of diorites, quartz diorites, granodiorites, monzogranites, and syenogranites (Tang et al., 2014). Late Triassic magmatic rocks are bimodal and includes gabbro-diorite, granodiorite, and syenogranites (Tang et al., 2016). Late Jurassic intrusives comprise monzogranites and syenogranites (Tang et al., 2016). To the south, Middle to Late Triassic volcanism in the Xing'an magmatic province is mostly mafic (basalts) but includes basaltic andesites, andesites, and dacites (Li et al., 2017). Widespread Middle Jurassic volcanism was bimodal and includes basalt, andesites, and basaltic andesites (Tamulan Formation; Li et al., 2015).

Igneous rocks from the Erguna and Xing'an magmatic provinces are mostly subalkaline (Figs. 3a,b), high-K calc-alkaline in the Early Triassic and medium to high-K calc-alkaline in the Middle Triassic. High silica samples have shoshonitic signatures (Fig. 3c,d). Rocks are primarily magnesian with subordinate ferroan compositions (Figs. 3e,f), metaluminous, and I-type, with secondarily S-type, and transition to A2-type magmatism in the Middle Triassic to Jurassic (Figs. 3g,h). Trace element data for samples from Early to Middle Permian and Middle Triassic to Middle Jurassic are reported (Fig. S2). There is, however, no data for late Permian to Early Triassic rocks. Samples from both provinces are enriched in LREE compared to HREE (Fig. S2). In details however, samples from these two magmatic provinces show more trace element variability. As an example, enriched samples ($Sr_N > 10$) from Middle Triassic in the Erguna province show positive anomalies in Ba, Pb, Zr and Hf. Such

anomalies are not observed in the Xing'an province for the same time period (Fig. S2). Similarly, a subgroup of the Early to Middle Jurassic samples in the Erguna province show significantly higher fractionation of HREE. Most depleted samples ($Sr_N < 10$) also show a negative Eu anomaly.

4.2. Isotopic Composition

Isotopic data for the magmatic provinces include Sm-Nd and Rb-Sr in whole rock and zircon Lu-Hf data (Figs. 2,4). Whole-rock Sm-Nd isotopic data is available for the OT-TB and, locally, for the Khangay Batholith and MGVB. In epsilon Nd notation

$$(\epsilon Nd(t) = \left[\frac{\left(\frac{^{143}Nd}{^{144}Nd} \right)_{sample}}{\left(\frac{^{143}Nd}{^{144}Nd} \right)_{CHUR}} - 1 \right] \times 10000,$$

with CHUR, the chondritic uniform reservoir), Permian to Triassic data are between -7.5 and +5 (Fig. 4c). Rb-Sr isotopic data are mainly available for the OT-TB and yields widespread $^{87}Sr/^{86}Sr$ ratios (Fig. 4d). Zircon Lu-Hf data are available for the batholiths and the Erguna and Xing'an magmatic provinces (Figs. 4a,b). In both regions, data are mainly enriched with respect to the bulk silica Earth

$$(\epsilon Hf(t) = \left[\frac{\left(\frac{^{176}Hf}{^{177}Hf} \right)_{sample}}{\left(\frac{^{176}Hf}{^{177}Hf} \right)_{CHUR}} - 1 \right] \times 10000 > 0;$$

Figs. 4a,b). Hf isotopic ratios in the Triassic batholiths have a narrower range than among Permian samples, whereas in the Xing'an magmatic province

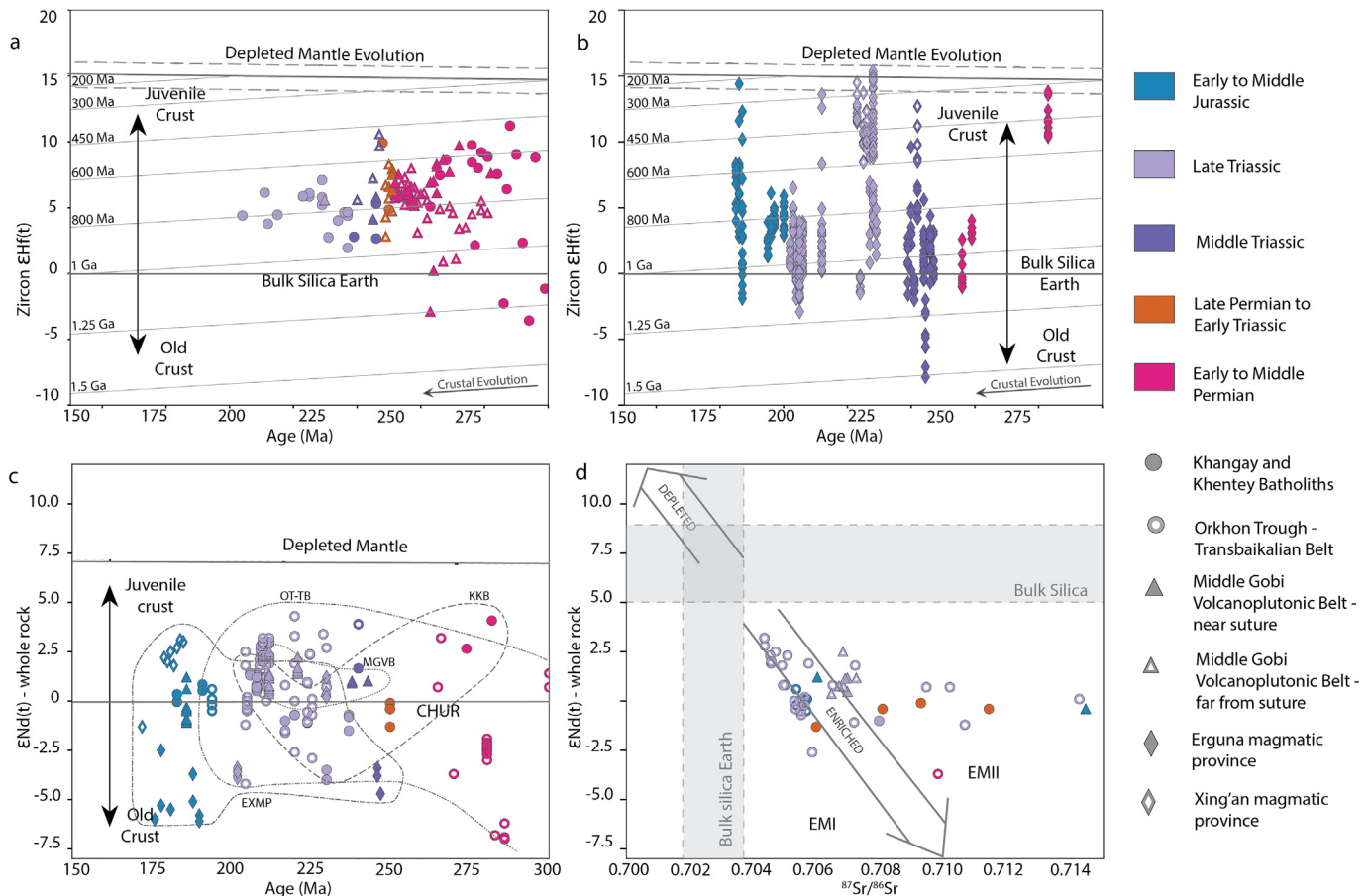


Figure 4. a) $\epsilon Hf(t)$ in detrital zircons vs age (Ma) from all samples in the western side (Khangay and Khentey batholiths and MGVB). b) Same as in A but for samples from the eastern side (Erguna and Xing'an magmatic provinces). c) $\epsilon Nd(t)$ for whole rock geochemistry and d) whole-rock $\epsilon Nd(t)$ vs $^{87}Sr/^{86}Sr$ for samples in the western magmatic belts. Dashed lines outlining data for magmatic provinces. OT-TB: Orkhon Trough-Transbaikalian Belt, KKB: Khangay and Khentey batholiths, MGVB: Middle Gobi Volcanoplutonic Belt, EXMP: Erguna and Xing'an Magmatic Provinces. Average crustal evolution based on $^{176}Lu/^{177}Hf = 0.0115$ (Vervoort et al., 1999).

(empty symbols, away from the suture) these values are more positive relative to most samples in the Erguna magmatic province (filled symbols, near the suture) (Figs. 4a,b). However, a few samples (Permian, Early Triassic, and Jurassic) in the Erguna magmatic province show values that are comparable to the positive values away from the suture (Fig. 4d).

5. Interpretation: Geochemical processes during magmatism

The analysis of the spatiotemporal geochemical trends north and south of the suture and along the suture provides important clues for understanding the first-order processes in the mantle and the crust that produced magmatism during the closure of the MOO. Our analysis is separated into two regions, one formed by the Khangay and Khentey batholiths, the OT-TB and the MGVB in the west, and one formed in the Erguna and Xing'an magmatic provinces in the east. Additionally, because assimilation of crustal rocks is a common process in continental convergent margins (e.g., Hildreth and Moorbath, 1988), the analysis below also considers signatures in mafic samples ($\text{SiO}_2 < 53\%$) which likely experienced negligible contamination.

5.1. Subduction Components

Subduction signatures in magmatic rocks include relative enrichment in fluid mobile elements (e.g., Ba, U, and large ion lithophile elements, LILE—Rb, K, Sr, and Pb) and Th, an element mobile in hydrous silicate melts, with respect to less fluid-mobile elements (Ti, and high field strength elements, HFSE—Nb, Ta, Hf, Zr, and Y) and of LREE (La to Sm) with respect to HREE (e.g., Lee et al., 2007; Mantle and Collins, 2008; Escrig et al., 2009; Zheng, 2019; Stern, 2020). Geochemical parameters in a subduction setting reflect a combination of slab contributions (e.g., LILE), mantle wedge contributions (e.g., HFSE and HREE), the effect of fractionation and partial melting (e.g., La, Y, Yb, Sr), magma mixing, and assimilation of crustal components (e.g., Profeta et al., 2015; Zheng, 2019). Additionally, both slab fluids and melts can be released from the slab to the mantle wedge (e.g., Elliott et al., 1997; Hochstaedter et al., 2001; Tollstrup et al., 2010; Hanyu et al., 2012; Shuto et al., 2015; Straub et al., 2015; Turner and Langmuir, 2022). In subduction magmatism, the enrichment of fluid-mobile incompatible elements over fluid-immobile compatible elements originates primarily in the mantle wedge from dehydration of metamorphic rocks in the slab (e.g., Zheng, 2019). Ratios of incompatible vs compatible elements also indicate fractionation or partial melting of minerals at different pressure and temperature conditions, such as plagioclase (e.g., Sr/Y; Chiaradia, 2015; Profeta et al., 2015), garnet (e.g., La/Yb, Tb/Yb; Profeta et al., 2015; Wu et al., 2002), phlogopite (Rb/Sr; e.g., Chen et al., 2020), amphiboles (e.g., La/Yb, Ba/Rb; Profeta et al., 2015; Chen et al., 2020), and lawsonite (e.g., Th/La; Wang et al., 2021b).

Several studies have recognized the enrichment in subduction components in the Mesozoic magmatism related to the Mongol-Okhotsk Ocean (e.g., Berzina et al., 2009; Donskaya et al., 2012, 2013; Munkhtsengel et al., 2007; Antipin et al., 2016). This can be observed in trace element data (Fig. S2) which show general positive anomalies in Rb, Th, U, and Pb, negative anomalies in Nb, Y, and Yb, and relative enrichment in LREE compared to HREE. Moreover, the majority of samples are also relatively enriched in Sr ($\text{Sr}_N > 10$) and Ba, and depleted in Ta (Fig. S2); evidencing the predominance of a subduction signature in all magmatic belts. However, this signature could be acquired from crustal contamination from a crust enriched in subduction components after a long-lived subduction system (e.g., Yarmolyuk et al., 2002; Tsygankov et al., 2017).

Lanthanum is highly incompatible and has low fluid-mobility, whereas Nb is compatible and is fluid immobile (Class et al., 2000). Thus, the La/Nb ratio can serve as a proxy for the source fertility where high La/Nb values point to a depleted mantle (e.g., Zamboni et al., 2016). However, incorporation of crustal components depleted in Nb with respect to La can increase the La/Nb ratio (Halder et al., 2021). Samples in the MOB are enriched in La/Nb ($\text{La/Nb} > 1$), which could result from either a depleted mantle or crustal assimilation (Fig. 5a). Samples with basaltic compositions ($\text{SiO}_2 < 53\%$; Fig. 5b), which are less influenced by differentiation and assimilation than higher silica samples, support an enrichment in La/Nb due to partial melting in the mantle rather than due to crustal assimilation.

Barium is a fluid-mobile element while Nb is considered as immobile. Hence Ba/Nb is a proxy for fluid enrichment in a subduction setting (Langmuir et al., 2006). Samples from the MOB show a general enrichment in Ba/Nb, especially near the suture, which supports a fluid input from the subducting slab (Fig. 5c). However, the enrichment in fluid mobile elements (responsible for the high Ba/Nb) is coupled with a moderate enrichment in melt mobile elements (responsible for high La/Sm). A high La/Sm can also reflect a higher proportion of subducted sediment in the source and, to a lesser extent, fractional crystallization and/or partial melting (Labanieh et al., 2012). We see that a mantle metasomatized by fluids derived from the subducted slab alone cannot explain the high La/Sm ratios observed in mafic samples (Fig. 5d) and data support the contribution of subduction-related hydrous melts. Thus, based on La/Nb, Ba/Nb, and La/Sm, the magmatism was affected by active or recently active subduction, at least in magmatic provinces with mafic composition (OT-TB, MGVB far from the suture and the Erguna – Xing'an magmatic provinces).

5.2. Slab Fluids and Hydrous Melts

Slab fluids are one of the most important controlling factors of magmatism in a subduction setting. The enrichment in Ba (a highly mobile element in aqueous fluids) relative to other less-fluid mobile elements such as Th and La (Ba/Th, and Ba/La) have successfully been used to identify the role of fluids (e.g., Woodhead et al., 2001; Pearce et al., 2005; Escrig et al., 2009; Hermann and Rubatto, 2009; Labanieh et al., 2012). Magmatic rocks in the western region of the MOB show a clear dichotomy in Ba/Th, with low values near the suture and high values away from the suture (Fig. 6a). In contrast, Ba/Th values from rocks in the eastern side do not show spatial or temporal zonation, suggesting a heterogeneous contribution of slab fluids and hydrous melts (Fig. 6b). The decrease of the Ba/Th during fractionation is negligible compared to the range observed in Fig. 6a (George et al., 2004). Hence, (1) the fact that the more mafic samples present the highest Ba/Th ratio (Fig. 6a) support a mantle origin, and (2), the proximal more differentiated samples must have a different source and/or assimilation of crustal components, as suggested in Fig. 5. These observations could explain the decrease of the Ba/Th ratio where the mantle component signature is diluted by the addition of crustal components that are usually much richer in incompatible trace elements. Thus, even a small proportion of assimilation would erase the mantle signature in incompatible elements. High Ba/Th ratios observed in distal samples until the Late Triassic to Early Jurassic support an interpretation that the contribution of hydrous melts played an important role at least in the OT-TB and MGVB.

Phlogopite and amphibole are common hydrous minerals in subduction systems which are sensitive to P-T conditions (e.g., Zheng et al., 2016; Zheng, 2019). Amphibole is stable at < 3.0 GPa and < 1000 to 1100 °C (Pargasite; e.g., Green et al., 2010) whereas phlogopite (Mg-rich biotite) is stable over a wider range of pressure and temperature conditions (< 6.0 GPa and < 1300 °C;

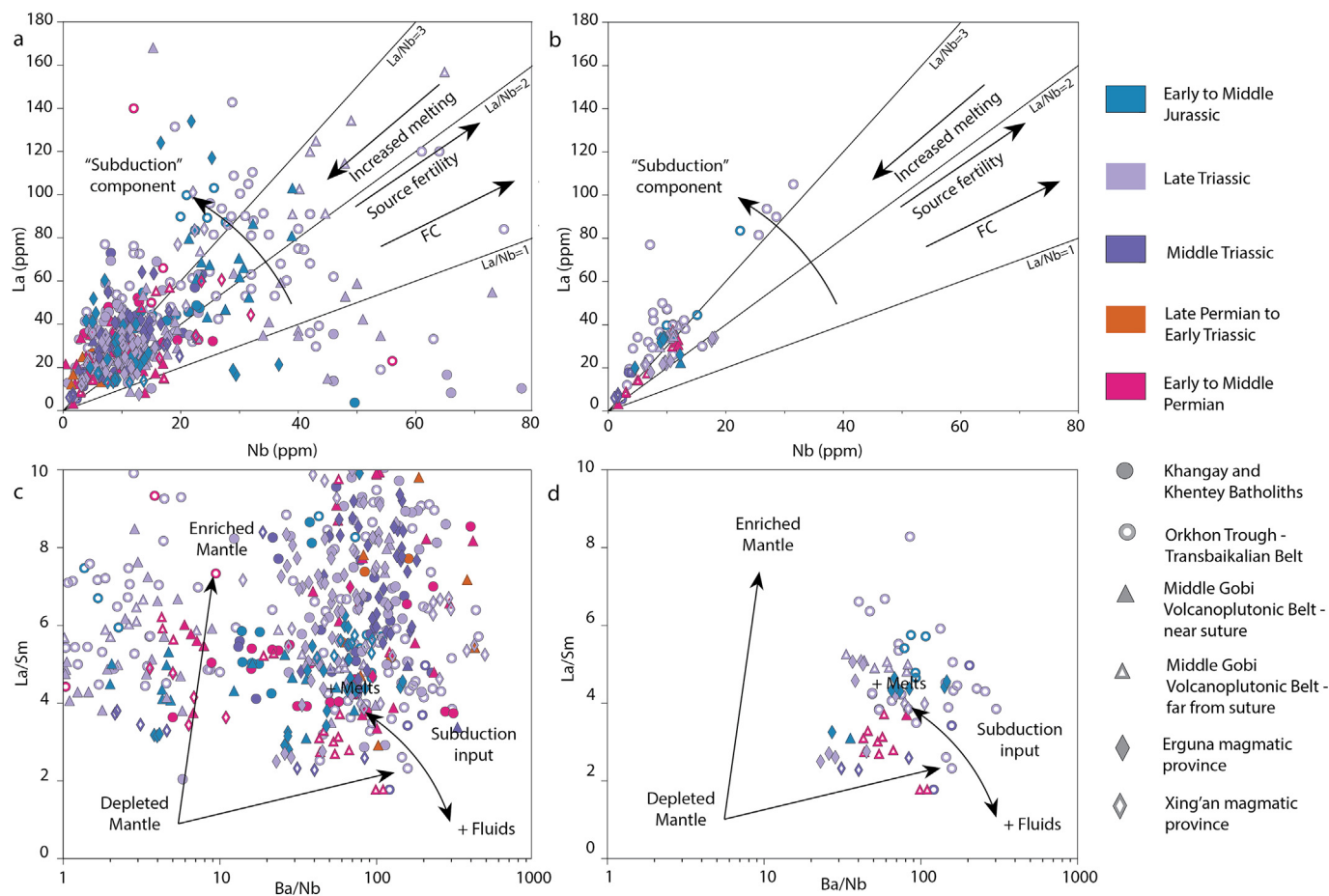


Figure 5. a-b) La vs. Nb (ppm) for all samples (a) and for mafic samples ($\text{SiO}_2 < 53\%$) (b). Modified from Allen et al. (2013). c-d) La/Sm vs. Ba/Nb for all samples (c) and for mafic samples (b). Modified from Langmuir et al. (2006).

Chen et al., 2020 and references therein). Rutile (TiO_2), a common accessory mineral in subduction zones and a major scavenger of HFSE such as Nb, Ta, and Ti (Zheng, 2019), is stable at shallow conditions and low thermal gradients (at $T < 1000$ °C for experimental melts produced at 3 GPa and with 7–15 wt.% H_2O and unstable in metasediments at $T > 1100$ °C; Zheng, 2019 and references therein). Partial melting of rutile-bearing rocks produces melts with high Nb/Ta ratios (e.g., Hermann and Rubatto, 2009), while partial melting in the presence of garnet produces high Gd/Yb in the melts (e.g., Qian and Hermann, 2013; Gómez-Tuena et al., 2018). On the other hand, partial melting of low-Mg amphibolite produces low Na/Ta melts (e.g., Foley et al., 2002). The Nb/Ta versus Rb/Ta diagram supports the interpretation of partial melting of an amphibole-rich source with some rutile in the residue, while the Gd/Yb versus Rb/Ta diagram also support the presence of some garnet in an amphibole-rich source (Fig. 6c). Hence, we conclude that amphibole (and not phlogopite) was the dominant hydrous phase in the subduction system. Moreover, Permian and Late Triassic samples from the OT-TB and early to middle Triassic samples from the Khangay Batholith show high Gd/Yb values, possibly due to partial melting of garnet in the source (Fig. 6d). The possible presence of garnet in the source is assessed in the following section.

5.3. Petrogenetic Processes

Petrogenetic processes in subduction settings include melting/dehydration of the oceanic slab, partial melting of a metasomatized mantle wedge, and assimilation/mixing and fractional crystalliza-

tion (AFC) within the crust (Wilson, 1989). In this section we focus on assessing the role of partial melting, fractional crystallization, and assimilation in the igneous geochemical record. Although this work aims to identify regional trends and the possible locations within the crust and mantle for the petrogenetic processes, the available data are heterogeneous, and their spatial distribution needs to be considered.

Element ratios such as Sr/Y and La/Yb can distinguish shallow fractionation, where Sr fractionates into plagioclase, from deep fractionation, where plagioclase is less stable (Sr is not fractionated) and HREE (including Y and Yb) fractionate into garnet (Profeta et al., 2015; Chiaradia, 2015). However, enrichment in La/Yb and Sr/Y can also result from fractionation out of residues rich in amphibole and/or garnet at the base of a thick crust (Castillo, 2012; Profeta et al., 2015; Chiaradia, 2015), partial melting of eclogites and garnet amphibolites (Castillo, 2012), and crustal contamination by sediments with high La/Yb ratios (e.g., Hanyu et al., 2006). Sr/Y versus Y, and (La/Yb) versus Yb plots (Figs. 7a,b) show low to high concentration of these ratios, although most samples near the suture (filled symbols in Figure 7) have higher values. Because samples near the suture tend to have higher silica content (which could result from crustal contamination), we focus on low silica samples. Mafic samples ($\text{SiO}_2 < 53\%$), only available for the Permian to Late Triassic in the OT-TB and Late Triassic to Early Jurassic in the Erguna magmatic province, show high Sr/Y and medium to high $(\text{La/Yb})_N$ values. Figure 7c also shows that the increase in Sr/Y and $(\text{La/Yb})_N$ is decoupled for low silica samples, which could result from partial melting of eclogites and garnet amphibolites derived from an oceanic slab (e.g., Umeda et al.,

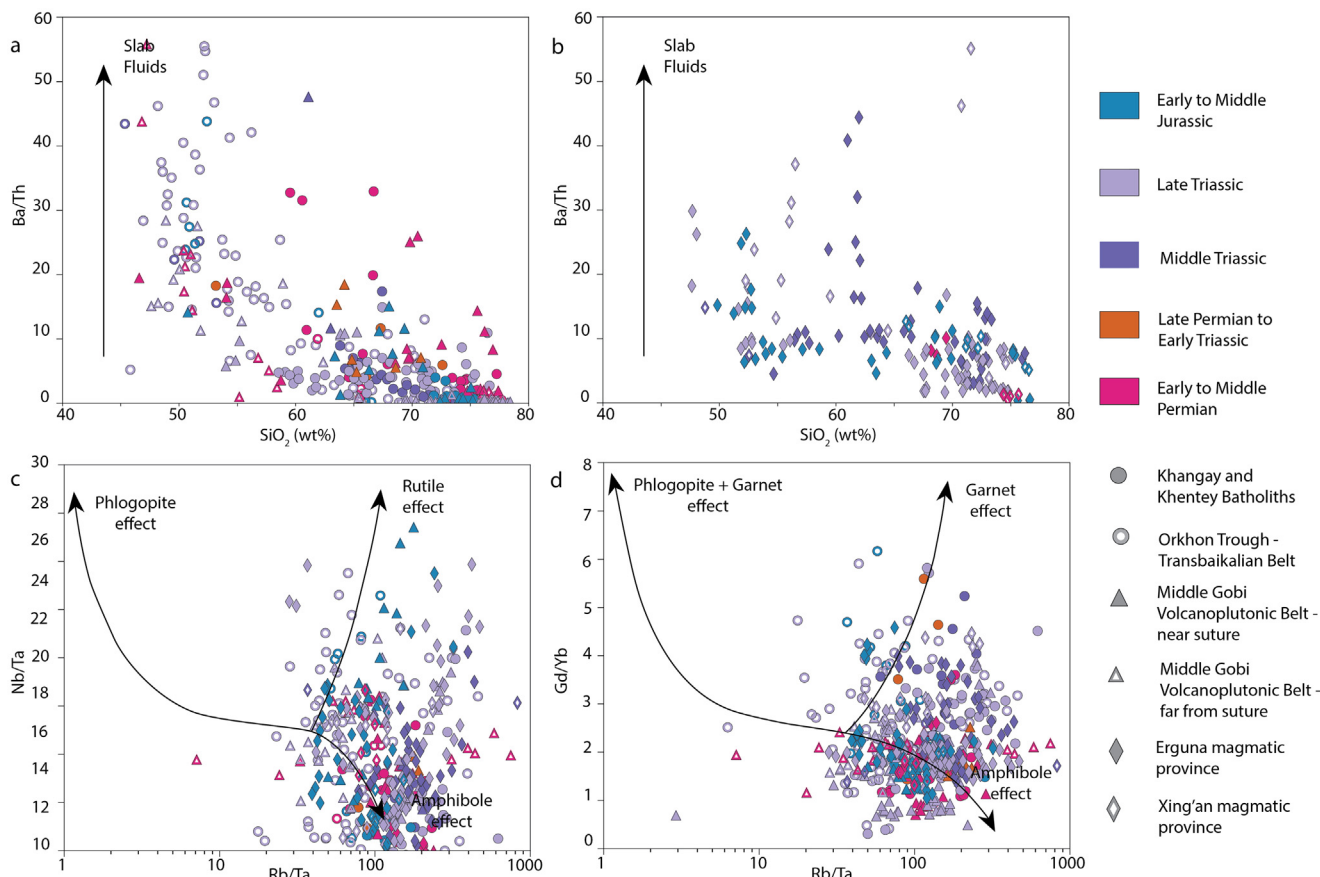


Figure 6. a-b) Ba/Th vs SiO₂ (wt%). A) for samples from the Khangay and Khentey batholiths, the MGVB, and the OT-TB, and b) from the Erguna and Xing'an magmatic provinces. c) Nb/Ta vs Rb/Ta and d) Gd/Yb vs Rb/Ta, are based on Gómez-Tuena et al. (2018). c-d) show data from all magmatic provinces.

2022) rather than from deep fractionation or crustal contamination. The $(La/Yb)_N$ versus La diagram for these mafic samples also support a compositional variability due to partial melting rather than fractional crystallization (Fig. 7e). When including all samples, the $(La/Yb)_N$ versus La diagram (Fig. 7d) shows that samples align with a partial melting trend especially near the trench, whereas samples away from the suture (i.e., open symbols) show combinations of both processes (partial melting and fractional crystallization). The La/Sm versus Sm diagram (Fig. 7f) also shows a partial melting trend and higher degrees of fractional crystallization in felsic samples from the MGVB and OT-TB (open symbols), consistent with magmatic differentiation playing a stronger role away from the suture. Moreover, distal high silica samples from the MGVB (open triangles) and, to a lesser extent, some samples from the OT-TB (open circles), show fractionation trends (Figs. 7d,f), low Sr values, and negative Eu anomalies (Fig. S2); these observations suggest low-pressure plagioclase fractionation in their petrogenesis. Although the Gd/Yb ratios support the presence of garnet in the source beneath the OT-TB and possibly beneath the Khangay Batholith during the Late Permian to Early Triassic (Fig. 6d), the later samples are high in silica, so crustal contamination and interaction with a deep cumulate during magma transport could be responsible for these high ratios. Thus, our major and trace element observations support a model in which distal samples to the north (in the OT-TB), record the contribution of a mantle metasomatized by hydrous melts likely derived from a slab rich in amphiboles and garnet, whereas distal samples to the south (in the MGVB) are strongly affected by fractional crystallization and likely assimilation processes.

Assimilation of crustal components can be better assessed with isotopic compositions and trace elements enriched in crustal components. One proxy for AFC is Rb/Nb versus Sr, where Rb/Nb increases with crustal components and Sr decreases with plagioclase fractionation (Halder et al., 2021). Magmatism in the western region of the MOB shows a clear dichotomy between proximal and distal samples from the suture zone. Most proximal samples (closed symbols in Fig. 7h) show both low Sr concentrations and high Rb/Nb ratios, consistent with an AFC process. Most distal samples (open symbols) show low Rb/Nb ratios for a wide range of Sr concentrations, suggesting a heterogeneous but significant degree of plagioclase fractionation. In NE China, samples near the suture are also enriched in Rb/Nb compared to samples far from the suture (Fig. 7i). Interestingly, the Rb/Nb ratios are, on average, higher west of the suture than east of the suture (Figs. 7h,i). This could reflect a west to east decrease in the influence of assimilation in their petrogenesis and/or in the Rb/Nb stored in the assimilated crust.

5.4. Sediment Melts

Sediment-derived melts are an important factor for the compositional range of magmas in active margins (e.g., Woodhead et al., 2001; Labanieh et al., 2012). Sediment melts produce crust-like patterns that are highly enriched in LILE, HFSE, LREE, and present high Th/La, Th/Yb, and Rb/Sr ratios (Förster et al., 2019). High Th/Yb is one of the main ratios associated with sediment melts (e.g., Woodhead et al., 2001; Hanyu et al., 2006); fractional crystallization, however, has the potential to increase this ratio (e.g.,

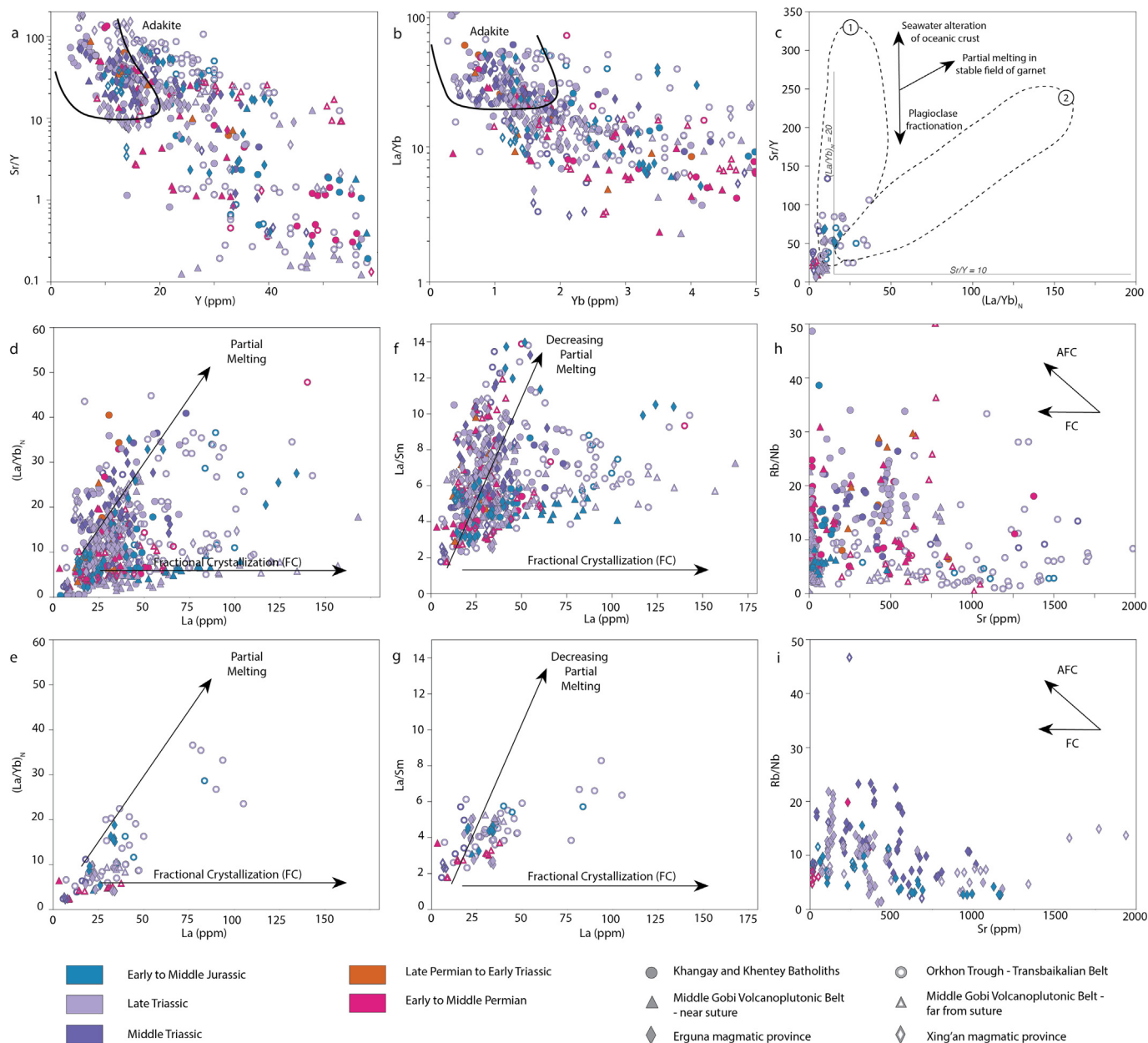


Figure 7. a) Sr/Y vs. Y (ppm) and b) (La/Yb) vs. Yb (ppm) modified from Drummond and Defant (1990). c) Sr/Y vs. (La/Yb)_N for SiO₂<53%. The field 1 is for oceanic-slab-derived adakites whereas Sr/Y is decoupled from (La/Yb)_N possibly due to seawater alteration; and field 2 is for deep fractionation at the base of a thick crust where Sr/Y and (La/Yb)_N concentrations are coupled (after Liu et al., 2010). d-e) (La/Yb)_N vs. La (ppm) for all samples (d) and for mafic samples (e) after Wang et al. (2008). f-g) La/Sm vs. La (ppm) for all samples (f) and for mafic samples (g) after Treuil and Joron (1975). (h-g) Rb/Nb vs. Sr (ppm) for samples from the Khangay and Khentey Batholiths and the MGVB (h) and from the Erguna and Xing'an magmatic provinces (g). Based on Halder et al. (2021).

Woodhead et al., 2001). Th/La is also commonly used to assess the role of sediment melts (e.g., Plank, 2005; Tommasini et al., 2011; Förster et al., 2019; Wang et al., 2021b), with high Th/La in magmatic arcs usually attributed as inherited from subducted sediments. The differentiation of the continental crust led to an enrichment in Th/La due to higher compatibility of La than Th in mafic and accessory minerals (Plank, 2005); thus, melts derived from the continental crust sediments are generally silica-rich and have high Th/La ratios. Finally, high Th/La (and low Sm/La) in potassic rocks can also be attributed to an enrichment of Th during post-collisional melting of blueschist mélanges formed at shallow depths in accretionary margins (Wang et al., 2021b).

Figure 8a shows that Th/Yb is generally enriched in all the magmatic provinces with values similar to those observed in some oceanic arcs (Lesser Antilles and Sunda arcs, Fig. 4 in Woodhead

et al., 2001); these high values may either suggest a strong influence from sediment melts or a significant effect of fractionation. As for other ratios describe above, the Th/La ratios between the distal and proximal zone in the western side of the suture are distinct (Fig. 8b). Samples near the suture have Th/La ratios that overlap with the terrigenous sediments range, average for the upper continental crust, and upper end of the marine sediment's value (Fig. 8b). Higher Th/La values generally correspond to samples more differentiated (i.e., highest SiO₂ content), however, proximal samples have higher Th/La values than distal samples regardless of the silica content. In contrast, the Th/La values in NE China are less variable and do not show differentiation between near and distal samples (Fig. 8c). On the other hand, except for a few samples from the OT-TB and MGVB that have higher values, most samples also show low Nb/U and Ce/Pb ratios (Fig. S3), consistently with a

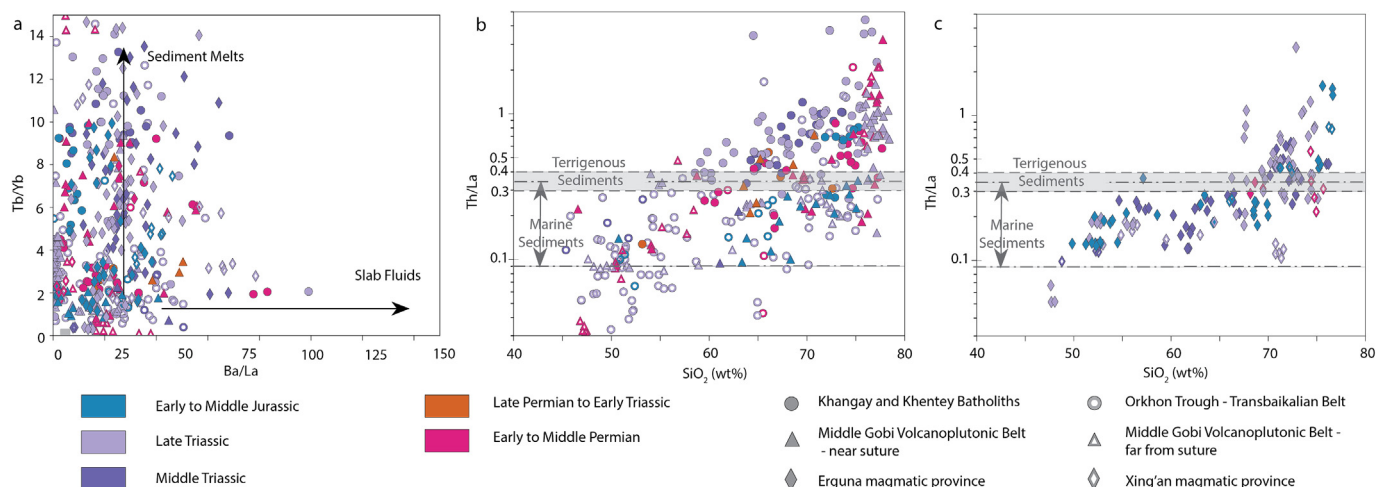


Figure 8. a) Th/Yb vs. Ba/La for all samples based on Woodhead et al. (2001). b-c) Th/La vs. SiO₂ (wt%) modified from Plank (2005). Th/La is variable in marine sediments (0.09–0.34) and elevated in continents (>0.25), especially in terrigenous sediments (0.3–0.4) (Plank, 2005). Values for the upper continental crust are 0.33 ± 0.05 and for the bulk continental crust are 0.27 ± 0.05 (Plank, 2005). Very high Th/La values (>0.5) are associated with magmatic differentiation while very low values (<0.1) with MORB (Plank, 2005) b) Th/La vs. SiO₂ (wt%) showing samples from the Khangay and Khentey batholiths and MGVB and c) showing samples from the Erguna and Xing'an magmatic provinces.

strong sedimentary signature (Elliott et al., 1997), and fall within the fields for GLOSS-II (global average of subducted sediment; Plank, 2014) and UCC (Upper Continental Crust; Rudnick and Gao, 2014) compositions.

In subduction systems, sediments can come from recycled marine sediments in the mantle source (slab sediments), relaminated sediments (or underplated) at the base of the crust (i.e., accretionary sediments, e.g., Hacker et al., 2011), or assimilated metasedimentary crust (i.e., contamination from crustal host rocks during magma transport). Marine sediments tend to have lower Th/La ratios than terrigenous sediments or the continental crust (Figs. 8b,c). We acknowledge that fractionation during melting depends on the mineralogy of the source; Pelletier et al. (2021), for instance, showed that the presence of monazite in the source can increase the Th/La ratio of the melt with monazite preferentially incorporating La over Th. However, to explain the largest offset between the samples proximal and distal from the suture (Fig. 8b) with the contribution of marine sediments alone would require both particularly enriched marine sediments and strong fractionation during melting. Limited geochemical data available for the proximal basement north of the suture has an average Th/La of ca. 0.32 (based on 13 clastic rocks from the Gorkhi Formation, Paleozoic accretionary complex; Hara et al., 2013), a value similar to the average upper continental crust (Th/La ca. 0.33; Fig. 8). In addition, while some samples from the western end of the suture have whole rock $\epsilon\text{Nd}(t)$ consistent with the contribution of an old crustal component, isotopic data other samples and detrital zircons show a signature of a juvenile crustal component (Fig. 4). Hence, the assimilation of an old basement to explain the high Th/La values alone is not supported by the isotopic data. Thus, we argue that both a contribution from relaminated sediments and contamination by the crustal basement are required to explain the isotopic and the trace element systematics in our samples, and that those contributions are higher near the suture and decreases abruptly away from the suture and more gradually toward the NE.

5.5. Crustal Sources

Isotopic data shown in Figure 4 indicate no major rejuvenation of the mantle, no true fertile magmas, and the involvement of Meso-Neoproterozoic crust. Isotopic data for the western mag-

matic provinces (Khangay and Khentey batholiths and MGVB; Fig. 4a) show that the basement rocks north and south of the suture are similar in age but that there is a change in the basement under the Khangay Batholith compared to the Khentey Batholith; this reveals a west to east zonation from a basement ca. 1.3 Ga–450 Ma under the Khangay Batholith to a basement ca. 1 Ga–600 Ma under the Khentey Batholith. In NE China, the same signature is recycled from the Permian to the Jurassic (Fig. 4b), suggesting a long-term magma reservoir at depth. Neodymium isotopic data available for the OT-TB (Figs. 4c,d) suggest the input of more juvenile components in the Late Triassic compared to the Permian. Additionally, it suggests that all samples have some level of crustal contamination hindering geochemical signatures related to the mantle source under the OT-TB. Moreover, the spread of $^{87}\text{Sr}/^{86}\text{Sr}$ data is consistent with contamination or assimilation of an old granitic crust. For this magmatic province (OT-TB), even though old crustal components are required to explain the isotopic values, the lack of zircon hafnium data hinders the assessment of possible juvenile contributions. Future zircon hafnium data will greatly improve the understanding of crustal components and mantle processes in the region.

6. Discussions

6.1. Mantle and crustal processes across and along the suture

The series of geochemical tracers and signatures presented in this study suggest a spatial and temporal variation in the magmatic belts/provinces across and along the suture.

6.1.1. Magmatism near the western end of the suture.

Magmatism in the western side of the suture varies systematically with the distance to the suture (Figs. 6, 7, and 8). Similar zonation in the slab fluids signatures, AFC, and sediment melt contributions is recorded north and south of the suture. These observations indicate subduction beneath both sides of the suture (e.g., Donskaya et al., 2012, 2013; Tang et al., 2014, 2016; Zhu et al., 2016; Liu et al., 2018; Sheldrick et al., 2020; Miao et al., 2020; Ganbat et al., 2021) and suggest some similarities in the mechanisms operating north and south of the suture.

In the interior magmatic belts (batholiths and part of the MGVB), evidence for higher AFC and sediment melt (Figs. 7h, 7i,

and 8a) is accompanied by relatively juvenile crustal components (Fig. 4), an eastward migration of magmatism, and no input of truly fertile mantle (Fig. 4). In the context of an eastward closing suture (modern coordinates), the proximity to sediments accumulated in the ocean basin next to the western end of the suture could have filled the trench and formed accretionary complexes that were later subducted. However, Mesozoic marine sediments along the MOB suture are scarcely preserved in the geologic record. One of the main melt components—especially near the western end of the suture—is sediment-derived melt. The sediment melt signature, which includes high K-calc-alkaline rocks (Figs. 3c and d) with high La/Sm (Fig. 5c), high Th/Yb (Fig. 8a), high Th/La (Figs. 8b,c), and low Ba/Th (6a,b), can result from the subduction of pelagic and terrestrial sediments (e.g., Zhu et al., 2019; Zhao et al., 2019) and crustal melts from metasediments (e.g., Zhao et al., 2017 and references therein). Crustal contamination from an accretionary complex, such as the ones that host the Khangay and Khentey batholiths (e.g., Kurihara et al., 2009), can also produce a sediment melt signature. However, evidence of AFC and sediment melts on the southern side of the suture where magmatism is not hosted on the Paleozoic accretionary complex suggests that contamination by the hosting accretionary rocks does not fully explain the strong sediment melt signature near the western edge of the suture. Moreover, even though the evidence for sedimentary components in the magmatism is clear, S-type granites are not common compared to I-types (Figs. 3g,h). This suggests that magmatism was not mainly formed by crustal anatexis, and rather was sourced from a mantle metasomatized by subduction-related fluids and melts. Thus, we propose that the sediment melts are at least partially linked to a sediment-rich margin and collision which provided sediments through subduction and underplating and/or relamination.

In the exterior magmatic belts, volcanic and intrusive rocks are compositionally bimodal, include I- and A-type magmatism (Figs. 3a, b, e, and f; e.g., Gerel and Munkhtsengel, 2004; Munkhtsengel et al., 2007; Donskaya et al., 2012, 2013; Machowiak and Stawikowski, 2012; Zhu et al., 2016), assimilated relatively juvenile crustal components with similar $\varepsilon Nd(t)$ values as the interior belts (Fig. 4c), present a strong subduction-derived geochemical signature regardless of silica content (Fig. 5), and show a significant contribution of slab-derived fluids (Fig. 6a). The strong signature of slab fluids and hydrous melts in the exterior belts (Figs. 5 and 6) suggest a metasomatized mantle at least until the Late Triassic and even Jurassic above the northern subduction margin (Figs. 5d and 6a). However, the exterior belts north and south of the suture have some striking differences. First, the southern belt (distal Middle Gobi Volcanoplutonic Belt) only was active during the Late Triassic while the OT-TB to the north was active from the Permian to the Early Jurassic (Figs. 2 and 3). The northern belt is longer, wider, and more voluminous (Fig. 2), and includes samples with adakitic compositions, possibly related to slab melts (Fig. 7c; e.g., Umeda et al., 2022). It also shows evidence for both partial melting and fractional crystallization (Fig. 7) processes. These differences suggest that the northern subduction zone was warmer and more metasomatized by subduction-related fluids than the southern subduction zone. This conclusion is consistent with a long-lived northward subduction system that accommodated the rotation of the margin that led to the closure of the basin as an orocline from the Permian to the time of closure compared to a stationary system to the south (e.g., Wang et al., 2021a).

6.1.2. Magmatism along the suture

Geochemical signatures along the suture reflect differences in the northern and southern margins during active subduction and basin closure. When comparing magmatism near the western trace

of the suture to magmatism in the eastern part of the MOB, both regions show higher AFC and higher contribution of sediment melts near the suture (Figs. 6a,b and 8). The AFC signature (Figs. 7h,i) and the Th/La ratio (Figs. 8 b,c), however, decrease from west to east along the suture, especially during the Triassic. We conclude that juvenile crust was assimilated along the whole suture (Figs. 4a,b) and it included younger components eastward along the suture. On the other hand, the role of slab fluids is more clear in both proximal and distal parts of the MOB from west to east (Figs. 6a,b). This suggests that the tectono-magmatic conditions and magma sources prevalent in the western magmatic belts changed to a more typical subduction system as the basin progressively closed to the east during the eastward closure of the MOO, at least along the southern side of the margin.

6.2. Magmatic Arc and Forearc Preservation in Central Mongolia

In this section, we use the modern distribution of magmatic rocks to discuss the location of the magmatic arc and the implications for the forearc preservation in central Mongolia.

Magmatism on the southeastern side of the suture shows evidence of an active margin above the south-directed subduction including the development of back-arc magmatism during the Late Triassic (e.g., Zhu et al., 2016; Sheldrick et al., 2020; Ganbat et al., 2022). The interpretation of back-arc extension is supported by the presence of a Late Permian ophiolite (Zhu et al., 2023). In this case, the arc is located immediately south of the suture, and most of what could be considered the forearc within the southern margin is apparently missing.

On the other hand, the tectono-magmatic conditions that led to the magmatism along the northern side of the suture are still debated. These interpretations are largely based on the magmatic record, however, geochemical characteristics of the magmatism are non-unique to a tectonic setting, and there is a lack of sedimentary and structural data documenting, for example, the presumed extensional setting for the OT-TB (e.g., Umeda et al., 2022). Despite this, the development of two distinctive magmatic belts prompts two tectonic scenarios. In the first scenario, an arc/back-arc model suggests that the exterior belt (OT-TB) was emplaced in a back-arc setting related to slab roll-back leading to the closure of the MOO (e.g., Xiao et al., 2018; Wang et al., 2021a). The batholiths represent a sediment-rich migrating arc until the Middle Triassic (e.g., Ganbat et al., 2021) or Late Triassic (e.g., Donskaya et al., 2013) while in the back-arc, slab processes, such as slab tear, break-off (e.g., Donskaya et al., 2013), or detachment could have facilitated the upwelling and melting of a mantle metasomatized by subduction-related fluids until the Late Triassic. In this scenario, the arc was emplaced in the Paleozoic accretionary complex, proximal to the suture zone, suggesting that a significant portion of the Permian to Triassic forearc rocks were removed during the collision. In the second scenario, the OT-TB records a relatively alkaline and fluid-rich arc magmatism until the Middle Triassic (e.g., Umeda et al., 2022) or Late Triassic (e.g., Donskaya et al., 2012), while near the suture, the batholiths record sediment-rich syn-collisional magmatism during the Middle Triassic (Khangay Batholith; Orolmaa et al., 2008) and post-orogenic to anorogenic magmatism in the Late Triassic (Khentey Batholith; Antipin et al., 2016). In this second scenario, the collision took place sometime in the Middle to Late Triassic, and the Paleozoic accretionary complex that hosts the batholiths sat in the forearc position until the collision. Contrary to the first scenario, the second scenario suggests the preservation of a significant part of the Permian to Middle Triassic forearc basement along the northern side of the suture. Beyond these scenarios, the preservation of the Paleozoic accretionary complex north of the suture combined with the evidence of a longer-lived subduction system on the northern side and the

limited forearc rocks along the southern margin support that the northern margin overrode the southern margin during the collision (Zorin, 1999).

6.3. Implications for crustal growth and amalgamation processes

Convergent margins are often linked to both crustal growth and crustal destruction, while collisional belts are linked to crustal preservation instead of continental production (e.g., Cawood et al., 2009). In non-collisional convergent margins, crustal growth happens when crustal addition - by incorporating fertile magmas and/or accreting island arcs to the margin - is greater than the crustal destruction - through recycling sediments back to the mantle (Cawood et al., 2009; Hawkesworth et al., 2016). Even though the crustal volume has been decreasing globally since the breakup of Rodinia (0.75 Ga), the preservation potential in otherwise destructive margins is greater in the final stages of subduction and collision (Hawkesworth et al., 2016).

ϵHf data show that the same juvenile crustal signature is being recycled in the magmatic arc at least since the Permian (Fig. 4). In the OT-TB, a slight increase in $\epsilon Hf(t)$ from the Permian to the Triassic supports the assimilation of more juvenile crustal materials. Similarly, more positive ϵHf values away from the suture in the Xing'an magmatic province shows the assimilation of more juvenile materials. Moreover, high degrees of crustal assimilation and sediment contributions in the magmatic record documented in this study highlight addition of crust via underplating, relamination, or material accreted along the margin.

Partial melting of sedimentary rocks such as the ones documented along the MOB usually requires high geothermal gradients, with temperatures at the subduction interface of ca. 200 °C higher than normal slabs (Hanyu et al., 2006). Processes that can help explain unusually high geothermal gradients include the age of the slab (younger slabs are warmer), low subduction rates and oblique subduction (by increasing the time to reheat), low subduction angle, and extremely high temperature conditions in the mantle wedge, for example, associated to a back-arc opening (Hanyu et al., 2006 and references therein). In the western region of the suture, the greater amount of sediment contributions and crustal melts to the magmatism without the systematic production of S-type intrusions suggest that the high geothermal gradients are due to asthenospheric upwelling, possibly related to slab roll-back or slab break-off during or immediately after the collision.

The combination of abundant sediments along the margin and a closing margin through subduction both north and south of the suture led to a sediment-rich collision that provided the conditions for recycling sediments back to the crust and differentiating and stabilizing a compositionally evolved crust. Thus, magmatism during the Permian and Triassic not only added mantle material to the crust, but also assimilated and preserved both sediments and juvenile crustal material formed in the Meso- and Neoproterozoic. These processes helped preserve and stabilize the crust along the convergent margin during the closure of the MOO.

7. Conclusions

The closure and final suturing of the Mongol-Okhotsk Ocean produced voluminous magmatic provinces north and south of the suture. Permian to Jurassic magmatism along the suture is enriched in fluid mobile elements (e.g., Ba, Pb), LILE (Rb, Th, K, Sr), and LREE (e.g., La, Ce) and is depleted in HFSE (e.g., Nb, Ta, Hf, Zr) and Y, and HREE. This enrichment in subduction components is observed north and south of the suture regardless of the silica content and thus is not solely produced by crustal contamination. We conclude that this attests to a mantle metasomatized

by slab-related hydrous melts and thus, to a both north and south-directed subduction (in modern coordinates) that led to the closure of the basin. Moreover, a larger volume, wider distribution, and more pronounced geochemical anomalies along the northern side of the suture are consistent with a longer-lived northward subduction system that accommodated significant part of the rotation leading to the closure of the Mongol Okhotsk Ocean compared to a smaller and more stationary system to the south (e.g., Wang et al., 2021a).

The influence of slab fluids is stronger in the distal magmatic belts near the western trace of the suture and in NE China. Hydrous melts are produced along this western suture segment and in NE China until the Jurassic, which indicates that the mantle was metasomatized by subduction related fluids either during active or recently active subduction. On the other hand, magmatic rocks within the western part of the suture are rich in sediment melt and crustal components without producing mainly S-type peraluminous magmatism. This implies mixing of mantle and crustal components as opposed to crustal anatexis. Isotopic data show that magmatism in the MOB recycled juvenile crustal components along the whole trace suture. Thus, this sediment-rich collision was able to recycle sediments back to the crust and contribute to crustal growth through stabilizing a younger and compositionally evolved crust in the core of the Central Asian Orogenic Belt.

Data Statement

The data and compilations used in this manuscript are available on Hive, an open-access repository for research data generated at the University of Utah:

<https://doi.org/10.7278/S50d-0phb-z0x0>

<http://doi.org/10.7278/S50d-fraf-ds5g>

CRediT authorship contribution statement

Henriquez Susana: Conceptualization, Methodology, Software, Validation, Formal analysis, Investigation, Data curation, Writing – original draft, Visualization. **Ochir Gerel:** Writing – review & editing, Supervision. **Lambart Sarah:** Writing – review & editing, Supervision. **L. Johnson Cari:** Writing – review & editing, Supervision, Project administration, Funding acquisition. **E. Webb Laura:** Writing – review & editing, Project administration, Funding acquisition. **C. Lippert Peter:** Writing – review & editing, Project administration, Funding acquisition.

Declaration of competing interest

The authors declare that they have no known competing financial interests or personal relationships that could have appeared to influence the work reported in this paper.

Acknowledgments

The authors are grateful to the National Science Foundation for funding this work (grant EAR-TECTONICS 1917645). SL also acknowledges funding support from NSF grant EAR-1946346. This work has benefited from discussions with Dr. Kurt Sundell. The authors appreciate the editorial handling by Dr. Yongjiang Liu and the constructive feedback from Dr. Shan Li and an anonymous reviewer which helped improve the manuscript.

Appendix A. Supplementary data

Supplementary data to this article can be found online at <https://doi.org/10.1016/j.gr.2024.07.015>.

References

- Allen, M.B., Kheirkhah, M., Neill, I., Emami, M.H., McLeod, C.L., 2013. Generation of Arc and Within-plate Chemical Signatures in Collision Zone Magmatism: Quaternary Lavas from Kurdistan Province, Iran. *J. Petrol.* 54 (5), 887–911. <https://doi.org/10.1093/petrology/egs090>.
- Antipin, V., Gerel, O., Perepelov, A., Odgerel, D., Zolboo, T., 2016. Late Paleozoic and Early Mesozoic rare-metal granites in Central Mongolia and Baikal region: Review of geochemistry, possible magma sources and related mineralization. *J. Geosci.* 105–125. <https://doi.org/10.3190/jgeosci.211>.
- Antipin, V.S., Perepelov, A.B., Odgerel, D., 2019. Rare-Metal Granites from Various Zones of the Early Mesozoic Magmatic Areal (Mongolia): Geochemical and Petrogenetic Features. *Doklady Earth Sci.* 485 (1), 317–321. <https://doi.org/10.1134/S1028334X19030267>.
- Arzhannikova, A.V., Demonterova, E.I., Jolivet, M., Mikheeva, E.A., Ivanov, A.V., Arzhannikov, S.G., Khubanov, V.B., Kamenetsky, V.S., 2022. Segmental closure of the Mongol-Okhotsk Ocean: Insight from detrital geochronology in the East Transbaikalia Basin. *Geosci. Front.* 13 (1), 101254. <https://doi.org/10.1016/j.gsf.2021.101254>.
- Badarch, G., Dickson Cunningham, W., Windley, B.F., 2002. A new terrane subdivision for Mongolia: Implications for the Phanerozoic crustal growth of Central Asia. *J. Asian Earth Sci.* 21 (1), 87–110. [https://doi.org/10.1016/S1367-9120\(02\)00017-2](https://doi.org/10.1016/S1367-9120(02)00017-2).
- Berzina, A.P., Gimón, V.O., Nikolaeva, I.V., Palesskii, S.V., Travin, A.V., 2009. Basites of the polychronous magmatic center with the Erdenetiyn-Ovoo porphyry Cu-Mo deposit (northern Mongolia): Petrogeochemistry, $^{40}\text{Ar}/^{39}\text{Ar}$ geochronology, geodynamic position, and related ore formation. *Russ. Geol. Geophys.* 50 (10), 827–841. <https://doi.org/10.1016/j.rgg.2009.09.001>.
- Castillo, P.R., 2012. Adakite petrogenesis. *Lithos* 134–135, 304–316. <https://doi.org/10.1016/j.lithos.2011.09.013>.
- Cawood, P.A., Kröner, A., Collins, W.J., Kusky, T.M., Mooney, W.D., Windley, B.F., 2009. Accretionary orogens through Earth history. *Geol. Soc. Lond. Special Publications* 318 (1), 1–36. <https://doi.org/10.1144/SP318.1>.
- Chen, L., Zheng, Y.-F., Zhao, Z.-F., 2020. Origin of arc-like magmatism at fossil convergent plate boundaries: Geochemical insights from Mesozoic igneous rocks in the Middle to Lower Yangtze Valley, South China. *Earth Sci. Rev.* 211, 103416. <https://doi.org/10.1016/j.earscirev.2020.103416>.
- Chiaradia, M., 2015. Crustal thickness control on Sr/Y signatures of recent arc magmas: An Earth scale perspective. *Sci. Rep.* 5 (1), 8115. <https://doi.org/10.1038/srep08115>.
- Class, C., Miller, D.M., Goldstein, S.L., Langmuir, C.H., 2000. Distinguishing melt and fluid subduction components in Umnak Volcanics, Aleutian Arc. *Geochem. Geophys. Geosyst.* 1 (6). <https://doi.org/10.1029/1999GC000010>.
- Daoudene, Y., Gapais, D., Ledru, P., Cocherie, A., Hocquet, S., Donskaya, T.V., 2009. The Ereendavaa Range (north-eastern Mongolia): An additional argument for Mesozoic extension throughout eastern Asia. *Int. J. Earth Sci.* 98 (6), 1381–1393. <https://doi.org/10.1007/s00531-008-0412-2>.
- Dash, B., Yin, A., Jiang, N., Tseveendorj, B., Han, B., 2015. Petrology, structural setting, timing, and geochemistry of Cretaceous volcanic rocks in eastern Mongolia: Constraints on their tectonic origin. *Gondwana Res.* 27 (1), 281–299. <https://doi.org/10.1016/j.gr.2013.10.001>.
- Donskaya, T.V., Gladkochub, D.P., Mazukabzov, A.M., De Waele, B., Presnyakov, S.L., 2012. The Late Triassic Kataev volcanoplutonic association in western Transbaikalia, a fragment of the active continental margin of the Mongol-Okhotsk Ocean. *Russ. Geol. Geophys.* 53 (1), 22–36. <https://doi.org/10.1016/j.rgg.2011.12.002>.
- Donskaya, T.V., Gladkochub, D.P., Mazukabzov, A.M., Ivanov, A.V., 2013. Late Paleozoic–Mesozoic subduction-related magmatism at the southern margin of the Siberian continent and the 150 million-year history of the Mongol-Okhotsk Ocean. *J. Asian Earth Sci.* 62, 79–97. <https://doi.org/10.1016/j.jseas.2012.07.023>.
- Drummond, M.S., Defant, M.J., 1990. A model for Trondhjemite-Tonalite-Dacite Genesis and crustal growth via slab melting: Archean to modern comparisons. *J. Geophys. Res. Solid Earth* 95 (B13), 21503–21521. <https://doi.org/10.1029/JB095iB13p21503>.
- Edel, J.B., Schulmann, K., Hanžl, P., Lexa, O., 2014. Palaeomagnetic and structural constraints on 90° anticlockwise rotation in SW Mongolia during the Permo-Triassic: Implications for Altaid oroclinal bending. Preliminary palaeomagnetic results. *J. Asian Earth Sci.* 94, 157–171. <https://doi.org/10.1016/j.jseas.2014.07.039>.
- Ehiro, M., Zakhro, Y., Minji, C., 2006. Early Triassic (Olenekian) ammonoids from Khentey Province, Mongolia, and their paleobiogeographic significance. *Bulletin Tohoku University Museum* 15.
- Elliott, T., Plank, T., Zindler, A., White, W., Bourdon, B., 1997. Element transport from slab to volcanic front at the Mariana arc. *J. Geophys. Res. Solid Earth* 102 (B7), 14991–15019. <https://doi.org/10.1029/97JB00788>.
- Escrig, S., Bézou, A., Goldstein, S.L., Langmuir, C.H., Michael, P.J., 2009. Mantle source variations beneath the Eastern Lau Spreading Center and the nature of subduction components in the Lau basin-Tonga arc system: Isotope geochemistry of lau basin lavas. *Geochem. Geophys. Geosyst.* 10 (4), n/a–n/a. <https://doi.org/10.1029/2008GC002281>.
- Foley, S., Tiepolo, M., Vannucci, R., 2002. Growth of early continental crust controlled by melting of amphibolite in subduction zones. *Nature* 417 (6891). <https://doi.org/10.1038/nature00799>.
- Förster, M.W., Prelević, D., Buhre, S., Mertz-Kraus, R., Foley, S.F., 2019. An experimental study of the role of partial melts of sediments versus mantle melts in the sources of potassic magmatism. *J. Asian Earth Sci.* 177, 76–88. <https://doi.org/10.1016/j.jseas.2019.03.014>.
- Fritzell, E.H., Bull, A.L., Shephard, G.E., 2016. Closure of the Mongol-Okhotsk Ocean: Insights from seismic tomography and numerical modelling. *Earth Planet. Sci. Lett.* 445, 1–12. <https://doi.org/10.1016/j.epsl.2016.03.042>.
- Frost, B.R., Barnes, C.G., Collins, W.J., Arculus, R.J., Ellis, D.J., Frost, C.D., 2001. A Geochemical Classification for Granitic Rocks. *J. Petrol.* 42 (11), 2033–2048. <https://doi.org/10.1093/petrology/42.11.2033>.
- Ganbat, A., Tsujimori, T., Miao, L., Safonova, I., Pastor-Galán, D., Anaad, C., Baatar, M., Aoki, S., Aoki, K., Savinskiy, I., 2021. Late Paleozoic–Early Mesozoic granitoids in the Khangay-Khentei basin, Central Mongolia: Implication for the tectonic evolution of the Mongol-Okhotsk Ocean margin. *Lithos* 404–405, 106455. <https://doi.org/10.1016/j.lithos.2021.106455>.
- Ganbat, A., Tsujimori, T., Miao, L., Safonova, I., Pastor-Galán, D., Anaad, C., Aoki, S., Aoki, K., Chimedsuren, M., 2022. Age, petrogenesis, and tectonic implications of the late Permian magmatic rocks in the Middle Gobi volcanoplutonic Belt, Mongolia. *Isl. Arc* e12457. <https://doi.org/10.1111/iar.12457>.
- Gerel, O., Munkhtsengel, B., 2004. Erdenetiin Ovoo porphyry copper–molybdenum deposit in northern Mongolia. *PGC Publishing* 20.
- George, R., Turner, S., Hawkesworth, C., Bacon, C.R., Nye, C., Stelling, P., Dreher, S., 2004. Chemical versus Temporal Controls on the Evolution of Tholeiitic and Calc-alkaline Magmas at Two Volcanoes in the Alaska–Aleutian Arc. *J. Petrol.* 45 (1), 203–219. <https://doi.org/10.1093/petrology/egg086>.
- Gerel, O., Batkhisig, B., Munkhtsengel, B., Javkhan, O., 2017. Geochemistry and geochronology of Mandalgovi Complex. *Mongolian Geoscientist* 48, 21–26. In Mongolian with English abstract.
- Gómez-Tuena, A., Mori, L., Straub, S.M., 2018. Geochemical and petrological insights into the tectonic origin of the Transmexican Volcanic Belt. *Earth Sci. Rev.* 183, 153–181. <https://doi.org/10.1016/j.earscirev.2016.12.006>.
- Green, D.H., Hibberson, W.O., Kovács, I., Rosenthal, A., 2010. Water and its influence on the lithosphere–asthenosphere boundary. *Nature* 467 (7314), 448–451. <https://doi.org/10.1038/nature09369>.
- Guo, Z.-X., Yang, Y.-T., Zybrev, S., Hou, Z.-H., 2017. Tectonostratigraphic evolution of the Mohe–Upper Amur Basin reflects the final closure of the Mongol-Okhotsk Ocean in the latest Jurassic–earliest Cretaceous. *J. Asian Earth Sci.* 145, 494–511. <https://doi.org/10.1016/j.jseas.2017.06.020>.
- Hacker, B.R., Kelemen, P.B., Behn, M.D., 2011. Differentiation of the continental crust by reamination. *Earth Planet. Sci. Lett.* 307 (3–4), 501–516. <https://doi.org/10.1016/j.epsl.2011.05.024>.
- Halder, M., Paul, D., Sensarma, S., 2021. Rhyolites in continental mafic Large Igneous Provinces: Petrology, geochemistry and petrogenesis. *Geosci. Front.* 12 (1), 53–80. <https://doi.org/10.1016/j.gsf.2020.06.011>.
- Han, J., Zhou, J.-B., Wang, B., Cao, J.-L., 2015. The final collision of the CAOB: Constraint from the zircon U–Pb dating of the Linxi Formation, Inner Mongolia. *Geosci. Front.* 6 (2), 211–225. <https://doi.org/10.1016/j.gsf.2014.06.003>.
- Hanyu, T., Tatsumi, Y., Nakai, S., Chang, Q., Miyazaki, T., Sato, K., Tani, K., Shibata, T., Yoshida, T., 2006. Contribution of slab melting and slab dehydration to magmatism in the NE Japan arc for the last 25 Myr: Constraints from geochemistry. *Geochem. Geophys. Geosyst.* 7 (8), 2005GC001220. <https://doi.org/10.1029/2005GC001220>.
- Hanyu, T., Gill, J., Tatsumi, Y., Kimura, J.-I., Sato, K., Chang, Q., Senda, R., Miyazaki, T., Hirahara, Y., Takahashi, T., Zulkarnain, I., 2012. Across- and along-arc geochemical variations of lava chemistry in the Sanghe arc: Various fluid and melt slab fluxes in response to slab temperature. *Geochem. Geophys. Geosyst.* 13 (10). <https://doi.org/10.1029/2012GC004346>.
- Hara, H., Kurihara, T., Tsukada, K., Kon, Y., Uchino, T., Suzuki, T., Takeuchi, M., Nakane, Y., Nuramkhaan, M., Chuluun, M., 2013. Provenance and origins of a Late Paleozoic accretionary complex within the Khangai-Khentei belt in the Central Asian Orogenic Belt, central Mongolia. *J. Asian Earth Sci.* 75, 141–157. <https://doi.org/10.1016/j.jseas.2013.07.019>.
- Hawkesworth, C.J., Cawood, P.A., Dhuime, B., 2016. Tectonics and crustal evolution. *GSA Today* 26 (09), 4–11. <https://doi.org/10.1130/GSATG272A.1>.
- Hermann, J., Rubatto, D., 2009. Accessory phase control on the trace element signature of sediment melts in subduction zones. *Chem. Geol.* 265 (3–4), 512–526. <https://doi.org/10.1016/j.chemgeo.2009.05.018>.
- Hildreth, W., Moorbath, S., 1988. Crustal contributions to arc magmatism in the Andes of Central Chile. *Contrib. Mineral. Petrol.* 98 (4), 455–489. <https://doi.org/10.1007/BF00372365>.
- Hochstaedter, A., Gill, J., Peters, R., Broughton, P., Holden, P., Taylor, B., 2001. Across-arc geochemical trends in the Izu-Bonin arc: Contributions from the subducting slab. *Geochem. Geophys. Geosyst.* 2 (7). <https://doi.org/10.1029/2000GC000105>.
- Jahn, B., Capdevila, R., Liu, D., Vernon, A., Badarch, G., 2004. Sources of Phanerozoic granitoids in the transect Bayanhongor–Ulaan Baatar, Mongolia: Geochemical and Nd isotopic evidence, and implications for Phanerozoic crustal growth. *J. Asian Earth Sci.* 23 (5), 629–653. [https://doi.org/10.1016/S1367-9120\(03\)00125-1](https://doi.org/10.1016/S1367-9120(03)00125-1).
- Jahn, B.M., Litvinovsky, B.A., Zanzivich, A.N., Reichow, M., 2009. Peralkaline granitoid magmatism in the Mongolian-Transbaikalian Belt: Evolution, petrogenesis and tectonic significance. *Lithos* 113 (3–4), 521–539. <https://doi.org/10.1016/j.lithos.2009.06.015>.
- Johnston, S., Weil, A., Gutierrez-Alonso, G., 2013. Oroclines: Thick and thin. *GSA Bull.* 125, 643–663. <https://doi.org/10.1130/B30765.1>.

- Jolivet, M., Arzhannikova, A., Frolow, A., Arzhannikov, S., Kulagina, N., Akulova, V., Vassallo, R., 2017. Late Jurassic - Early Cretaceous paleoenvironmental evolution of the Transbaikalian basins (SE Siberia): Implications for the Mongol-Okhotsk orogeny. *Bull. Soc. Géol. France* 188 (1–2), 9. <https://doi.org/10.1051/bsgf/2017010>.
- Kelty, T.K., Yin, A., Dash, B., Gehrels, G.E., Ribeiro, A.E., 2008. Detrital-zircon geochronology of Paleozoic sedimentary rocks in the Hangay-Hentey basin, north-central Mongolia: Implications for the tectonic evolution of the Mongol-Okhotsk Ocean in central Asia. *Tectonophysics* 451 (1–4), 290–311. <https://doi.org/10.1016/j.tecto.2007.11.052>.
- Khain, E., 2003. The Palaeo-Asian ocean in the Neoproterozoic and early Palaeozoic: New geochronological data and palaeotectonic reconstructions. *Precambrian Res.* 122 (1–4), 329–358. [https://doi.org/10.1016/S0301-9268\(02\)00218-8](https://doi.org/10.1016/S0301-9268(02)00218-8).
- Kilian, T.M., Swanson-Hysell, N.L., Bold, U., Crowley, J., Macdonald, F.A., 2016. Paleomagnetism of the Teel basalts from the Zavkhan terrane: Implications for Paleozoic paleogeography in Mongolia and the growth of continental crust. *Lithosphere* 8 (6), 699–715. <https://doi.org/10.1130/L552.1>.
- Kovalenko, V. I., Kuz'min, M. I., & Antipin, V. S. (1984). Mesozoic magmatism of the Mongolian-Okhotsk Belt and the possible geodynamic interpretation. *Int. Geol. Rev.*
- Kozlovsky, A.M., Salmikova, E.B., Yarmolyuk, V.V., Ivanova, A.A., Savatenkov, V.M., Plotkina, J.V., Oyunchimeg, T., 2023. Late Paleozoic alkaline granitoids of the southwestern and Northern Mongolia: U-Pb ID-TIMS zircon dating, petrogenesis and implications for post-accretion and anorogenic activity of the Central Asian Orogenic Belt. *Gondwana Res.* 121, 92–117. <https://doi.org/10.1016/j.gr.2023.04.007>.
- Kurihara, T., Tsukada, K., Otoh, S., Kashiwagi, K., Chuluun, M., Byambadash, D., Boijir, B., Gonchigdorj, S., Nuramkhan, M., Niwa, M., Tokiwa, T., Hikichi, G., Kozuka, T., 2009. Upper Silurian and Devonian pelagic deep-water radiolarian chert from the Khangai-Khentei belt of Central Mongolia: Evidence for Middle Paleozoic subduction-accretion activity in the Central Asian Orogenic Belt. *J. Asian Earth Sci.* 34 (2), 209–225. <https://doi.org/10.1016/j.jseae.2008.04.010>.
- Kuz'min, M. I., Yarmolyuk, V. V., & Kravchinsky, V. A. (2011). Phanerozoic within-plate magmatism of North Asia: Absolute paleogeographic reconstructions of the African large low-shear-velocity province. *Geotectonics*, 45(6), 415–438. Doi: 10.1134/S0016852111060045
- Labanih, S., Chauvel, C., Germa, A., Quidelleur, X., 2012. Martinique: A Clear Case for Sediment Melting and Slab Dehydration as a Function of Distance to the Trench. *J. Petrol.* 53 (12), 2441–2464. <https://doi.org/10.1093/ptrology/egs055>.
- Langmuir, C. H., Bézous, A., Escrig, S., & Parman, S. W., 2006. Chemical systematics and hydrous melting of the mantle in back-arc basins. In D. M. Christie, C. R. Fisher, S.-M. Lee, & S. Givens (Eds.), *Geophys. Monogr.* (Vol. 166, pp. 87–146). AGU. Doi: 10.1029/166GM07
- Large, R.R., 2001. The Alteration Box Plot: A Simple Approach to Understanding the Relationship between Alteration Mineralogy and Lithochemistry Associated with Volcanic-Hosted Massive Sulfide Deposits. *Econ. Geol.* 96 (5), 957–971. <https://doi.org/10.2113/96.5.957>.
- Lee, C.-T.-A., Morton, D.M., Kistler, R.W., Baird, A.K., 2007. Petrology and tectonics of Phanerozoic continent formation: From island arcs to accretion and continental arc magmatism. *Earth Planet. Sci. Lett.* 263 (3–4), 370–387. <https://doi.org/10.1016/j.epsl.2007.09.025>.
- Li, S.-C., Liu, Z.-H., Xu, Z.-Y., Li, G., Zhang, C., 2015. Age and tectonic setting of volcanic rocks of the Tamulangou Formation in the Great Xing'an Range, NE China. *J. Asian Earth Sci.* 113, 471–480. <https://doi.org/10.1016/j.jseae.2014.09.014>.
- Li, L., Sun, F., Li, B., Xu, Q., Zhang, Y., Qian, Y., 2016. Early Mesozoic Southward Subduction of the Eastern Mongol-Okhotsk Oceanic Plate: Evidence from Zircon U-Pb-Hf Isotopes and Whole-rock Geochemistry of Triassic Granitic Rocks in the Mohe Area, NE China: Mongol-Okhotsk ocean. Southward subduction. *Resour. Geol.* 66 (4), 386–403. <https://doi.org/10.1111/rge.12106>.
- Li, P., Sun, M., Narantsetseg, T., Jourdan, F., Hu, W., Yuan, C., 2022. First structural observation around the hinge of the Mongolian Orocline (Central Asia): Implications for the geodynamics of oroclinal bending and the evolution of the Mongol-Okhotsk Ocean. *GSA Bull.* <https://doi.org/10.1130/B36200.1>.
- Li, S., Wang, T., Wilde, S.A., Tong, Y., 2013. Evolution, source and tectonic significance of Early Mesozoic granitoid magmatism in the Central Asian Orogenic Belt (central segment). *Earth Sci. Rev.* 126, 206–234. <https://doi.org/10.1016/j.jseae.2013.06.001>.
- Li, Y., Xu, W.-L., Wang, F., Pei, F.-P., Tang, J., Zhao, S., 2017. Triassic volcanism along the eastern margin of the Xing'an Massif, NE China: Constraints on the spatial-temporal extent of the Mongol-Okhotsk tectonic regime. *Gondwana Res.* 48, 205–223. <https://doi.org/10.1016/j.gr.2017.05.002>.
- Liu, S.-A., Li, S., He, Y., Huang, F., 2010. Geochemical contrasts between early Cretaceous ore-bearing and ore-barren high-Mg adakites in central-eastern China: Implications for petrogenesis and Cu–Au mineralization. *Geochim. Cosmochim. Acta* 74 (24), 7160–7178. <https://doi.org/10.1016/j.gca.2010.09.003>.
- Liu, H., Li, Y., He, H., Huangfu, P., Liu, Y., 2018. Two-phase southward subduction of the Mongol-Okhotsk oceanic plate constrained by Permian–Jurassic granitoids in the Erguna and Xing'an massifs (NE China). *Lithos* 304–307, 347–361. <https://doi.org/10.1016/j.lithos.2018.01.016>.
- Machowiak, K., Stawikowski, W., 2012. The Baga-Gazriin Chuluu A-type granites of Central Mongolia compared with other igneous bodies nearby: A geochemical approach. *GEOL. Q.* 56 (3), 457–474. <https://doi.org/10.7306/gq.1033>.
- Maniar, P.D., Piccoli, P.M., 1989. Tectonic discrimination of granitoids. *GSA. Bull.* 101 (5), 635–643. [https://doi.org/10.1130/0016-7606\(1989\)101<0635:TDOG>2.3.CO;2](https://doi.org/10.1130/0016-7606(1989)101<0635:TDOG>2.3.CO;2).
- Mantle, G.W., Collins, W.J., 2008. Quantifying crustal thickness variations in evolving orogens: Correlation between arc basalt composition and Moho depth. *Geology* 36 (1), 87. <https://doi.org/10.1130/G24095A.1>.
- Meng, Q.-R., Hu, J.-M., Jin, J.-Q., Zhang, Y., Xu, D.-F., 2003. Tectonics of the late Mesozoic wide extensional basin system in the China–Mongolia border region: Wide extensional basin system. *Basin Res.* 15 (3), 397–415. <https://doi.org/10.1046/j.1365-2117.2003.00209.x>.
- Miao, L., Fan, W., Liu, D., Zhang, F., Shi, Y., Guo, F., 2008. Geochronology and geochemistry of the Hegenshan ophiolitic complex: Implications for late-stage tectonic evolution of the Inner Mongolia-Daxinganling Orogenic Belt, China. *J. Asian Earth Sci.* 32 (5–6), 348–370. <https://doi.org/10.1016/j.jseae.2007.11.005>.
- Miao, L., Zhu, M., Liu, C., Baatar, M., Anaad, C., Yang, S., Li, X., 2020. Detrital-Zircon Age Spectra of Neoproterozoic–Paleozoic Sedimentary Rocks from the Erendavaa Terrane in NE Mongolia: Implications for the Early-Stage Evolution of the Erendavaa Terrane and the Mongol-Okhotsk Ocean. *Minerals* 10 (9), 742. <https://doi.org/10.3390/min10090742>.
- Middlemost, E.A.K., 1994. Naming materials in the magma/igneous rock system. *Earth Sci. Rev.* 37 (3–4), 215–224. [https://doi.org/10.1016/0012-8252\(94\)90029-9](https://doi.org/10.1016/0012-8252(94)90029-9).
- Munkhtsengel, B., Gerel, O., Tsuchiya, N., Ohara, M., 2007. Petrochemistry of Igneous Rocks in Area of the Erdenetiin Oovo Porphyry Cu-Mo Mineralized District, Northern Mongolia. *AIP Conf. Proc.* 898, 63–65. <https://doi.org/10.1063/1.2721250>.
- Nakakuki, T., Mura, E., 2013. Dynamics of slab rollback and induced back-arc basin formation. *Earth Planet. Sci. Lett.* 361, 287–297. <https://doi.org/10.1016/j.epsl.2012.10.031>.
- Onon, G., Tsukada, K., 2017. Late Paleozoic low-angle southward-dipping thrust in the Züünharaa area, Mongolia: Tectonic implications for the geological structures in the Sayan-Baikal and Hangai-Daur belts. *Int. J. Earth Sci.* 106 (7), 2549–2573. <https://doi.org/10.1007/s00531-017-1446-0>.
- Orolmaa, D., Erdenesaihan, G., Borisenko, A.S., Fedoseev, G.S., Babich, V.V., Zhmodik, S.M., 2008. Permian-Triassic granitoid magmatism and metallogeny of the Hangay (central Mongolia). *Russ. Geol. Geophys.* 49 (7), 534–544. <https://doi.org/10.1016/j.rgg.2008.06.008>.
- Parfenov, L. M., Badarch, G., Berzin, N.A., Hwang, D. H., Khanchuk, A. I., Kuz'min, M. I., Nokleberg, W. J., Obolenskiy, A. A., Ogasawara, M., Prokopiev, A., Rodionov, N. V., Smelov, A. P., & Hongquan, Y. (2010). Metallogenesis and tectonics of northeast Asia. In *Metallogenesis and tectonics of northeast Asia* (p. 1.1-1.36). U.S. Geol. Surv. Prof. Pap. 1765. <http://pubs.er.usgs.gov/publication/pp17659>
- Pearce, J.A., Stern, R.J., Bloomer, S.H., Fryer, P., 2005. Geochemical mapping of the Mariana arc-basin system: Implications for the nature and distribution of subduction components. *Geochem. Geophys. Geosyst.* 6 (7). <https://doi.org/10.1029/2004GC000895>.
- Peccherillo, A., Taylor, S.R., 1976. Geochemistry of eocene calc-alkaline volcanic rocks from the Kastamonu area. Northern Turkey. *Contrib. Mineral Petrol.* 58 (1), 63–81. <https://doi.org/10.1007/BF00384745>.
- Pelleter, A.-A., Prouteau, G., Scaillet, B., 2021. The Role of Sulphur on the Melting of Ca-Poor Sediment and on Trace Element Transfer in Subduction Zones: An Experimental Investigation. *J. Petrol.* 62 (9), 1–42. <https://doi.org/10.1093/ptrology/egab005>.
- Plank, T., 2005. Constraints from Thorium/Lanthanum on Sediment Recycling at Subduction Zones and the Evolution of the Continents. *J. Petrol.* 46 (5), 921–944. <https://doi.org/10.1093/ptrology/egi005>.
- Plank, T., 2014. The Chemical Composition of Subducting Sediments. In: Holland, H. D., Turekian, K.K. (Eds.), *Treatise on Geochemistry*. (Second Edition), Elsevier, pp. 607–629. <https://doi.org/10.1016/B978-0-08-095975-7.00319-3>.
- Profeta, L., Ducea, M.N., Chapman, J.B., Paterson, S.R., Gonzales, S.M.H., Kirsch, M., Petrescu, L., DeCelles, P.G., 2015. Quantifying crustal thickness over time in magmatic arcs. *Sci. Rep.* 5 (1), 17786. <https://doi.org/10.1038/srep17786>.
- Qian, Q., Hermann, J., 2013. Partial melting of lower crust at 10–15 kbar: Constraints on adakite and TTG formation. *Contrib. Mineral Petrol.* 165 (6), 1195–1224. <https://doi.org/10.1007/s00410-013-0854-9>.
- Reichow, M.K., Litvinovsky, B.A., Parrish, R.R., Saunders, A.D., 2010. Multi-stage emplacement of alkaline and peralkaline syenite–granite suites in the Mongolian-Transbaikalian Belt, Russia: Evidence from U-Pb geochronology and whole rock geochemistry. *Chem. Geol.* 273 (1–2), 120–135. <https://doi.org/10.1016/j.chemgeo.2010.02.017>.
- Ritts, B.D., Berry, A.K., Johnson, C.L., Darby, B.J., Davis, G.A., 2010. Early Cretaceous supradetachment basins in the Hohhot metamorphic core complex, Inner Mongolia, China. *Basin Res.* 22 (1), 45–60. <https://doi.org/10.1111/j.1365-2117.2009.00433.x>.
- Rudnick, R.L., Gao, S., 2014. *Composition of the Continental Crust*. In: Holland, H.D., Turekian, K.K. (Eds.), *Treatise on geochemistry* Vol. 4, 1–51.
- Schellart, W.P., 2004. Kinematics of subduction and subduction-induced flow in the upper mantle. *J. Geophys. Res. Solid Earth* 109 (B7). <https://doi.org/10.1029/2004JB002970>.
- Sengör, A.M.C., Natal'in, B., 1994. *Paleotectonics of Asia: Fragments of a synthesis. The Tectonic Evolution of Asia*, 486–640.
- Sengör, A.M.C., Natal'in, B. A., & Burtman, V. S. 1993. Evolution of the Altai tectonic collage and Palaeozoic crustal growth in Eurasia. *Nature* 364 (6435), 299–307. <https://doi.org/10.1038/364299a0>.

- Sheldrick, T.C., Barry, T.L., Millar, I.L., Barfod, D.N., Halton, A.M., Smith, D.J., 2020. Evidence for southward subduction of the Mongol–Okhotsk oceanic plate: Implications from Mesozoic adakitic lavas from Mongolia. *Gondwana Res.* 79, 140–156. <https://doi.org/10.1016/j.gr.2019.09.007>.
- Shuto, K., Nohara-Imanaka, R., Sato, M., Takahashi, T., Takazawa, E., Kawabata, H., Takanashi, K., Ban, M., Watanabe, N., Fujibayashi, N., 2015. Across-arc Variations in Geochemistry of Oligocene to Quaternary Basalts from the NE Japan Arc: Constraints on Source Composition, Mantle Melting and Slab Input Composition. *J. Petrol.* 56 (11), 2257–2297. <https://doi.org/10.1093/ptrology/egv073>.
- Sorokin, A.A., Zaika, V.A., Kovach, V.P., Kotov, A.B., Xu, W., Yang, H., 2020. Timing of closure of the eastern Mongol–Okhotsk Ocean: Constraints from U–Pb and Hf isotopic data of detrital zircons from metasediments along the Dzhangdy Transect. *Gondwana Res.* 81, 58–78. <https://doi.org/10.1016/j.gr.2019.11.009>.
- Stern, C.R., 2020. The role of subduction erosion in the generation of Andean and other convergent plate boundary arc magmas, the continental crust and mantle. *Gondwana Res.* 88, 220–249. <https://doi.org/10.1016/j.gr.2020.08.006>.
- Straub, S.M., Woodhead, J.D., Arculus, R.J., 2015. Temporal Evolution of the Mariana Arc: Mantle Wedge and Subducted Slab Controls Revealed with a Tephra Perspective. *J. Petrol.* 56 (2), 409–439. <https://doi.org/10.1093/ptrology/egv005>.
- Tang, J., Xu, W.-L., Wang, F., Wang, W., Xu, M.-J., Zhang, Y.-H., 2014. Geochronology and geochemistry of Early–Middle Triassic magmatism in the Erguna Massif, NE China: Constraints on the tectonic evolution of the Mongol–Okhotsk Ocean. *Lithos* 184–187, 1–16. <https://doi.org/10.1016/j.lithos.2013.10.024>.
- Tang, J., Xu, W.-L., Wang, F., Zhao, S., Wang, W., 2016. Early Mesozoic southward subduction history of the Mongol–Okhotsk oceanic plate: Evidence from geochronology and geochemistry of Early Mesozoic intrusive rocks in the Erguna Massif, NE China. *Gondwana Res.* 31, 218–240. <https://doi.org/10.1016/j.gr.2014.12.010>.
- Tollstrup, D., Gill, J., Kent, A., Prinkey, D., Williams, R., Tamura, Y., Ishizuka, O., 2010. Across-arc geochemical trends in the Izu–Bonin arc: Contributions from the subducting slab, revisited. *Geochim. Geophys. Geosyst.* 11 (1). <https://doi.org/10.1029/2009GC002847>.
- Tommasini, S., Avanzinelli, R., Conticelli, S., 2011. The Th/La and Sm/La conundrum of the Tethyan realm lamproites. *Earth Planet. Sci. Lett.* 301 (3–4), 469–478. <https://doi.org/10.1016/j.epsl.2010.11.023>.
- Tomurtogoo, O., Windley, B.F., Kröner, A., Badarch, G., Liu, D.Y., 2005. Zircon age and occurrence of the Adaaatsag ophiolite and Muron shear zone, central Mongolia: Constraints on the evolution of the Mongol–Okhotsk ocean, suture and orogen. *J. Geol. Soc.* 162 (1), 125–134. <https://doi.org/10.1144/0016-764903-146>.
- Treuil, M., Joron, 1975. Utilisation des elements hygromagmatophiles pour la simplification de la modelisation quantitative del processus magmatiques. Exemples de l'afar er de la dorsale medio atlantique. *Societa Italiana Mineralogia e Petrologia*, 125–174.
- Tsukada, K., Umeda, K., Madmid, B., Sodnom, K., Nakuramkhaan, M., 2022. Ages from the “Mogod Formation” of the Permian–Triassic igneous rocks in the Sayan–Baikal belt, northern Mongolia. *Bull. Nagoya Univ. Museum*. <https://doi.org/10.18999/bulnum.037.01>.
- Tsygankov, A.A., Burmakina, G.N., Khabunov, V.B., Buyantuev, M.D., 2017. Geodynamics of Late Paleozoic batholith-forming processes in western Transbaikalia. *Petrol.* 25 (4), 396–418. <https://doi.org/10.1134/S0869591117030043>.
- Turner, S.J., Langmuir, C.H., 2022. A quantitative framework for global variations in arc geochemistry. *Earth Planet. Sci. Lett.* 584, 117411. <https://doi.org/10.1016/j.epsl.2022.117411>.
- Umeda, K., Purevsuren, N., Tsukada, K., Altansukh, L., Nadmid, B., Sodnom, K., Nuramkhaan, M., Kabashima, T., Kondo, T., 2022. Permian–Triassic adakitic igneous activity at Northern Mongolia: Implication for Permian–Triassic subduction system at the Siberian continental margin. *J. Geodyn.* 151, 101918. <https://doi.org/10.1016/j.jog.2022.101918>.
- Van der Voo, R., van Hinsbergen, D.J.J., Domeier, M., Spakman, W., Torsvik, T.H., 2015. Latest Jurassic–earliest Cretaceous closure of the Mongol–Okhotsk Ocean: A paleomagnetic and seismological–tomographic analysis. *Geol. Soc. Am. Spec.* 513, 589–606. [https://doi.org/10.1130/2015.2513\(19\)](https://doi.org/10.1130/2015.2513(19)).
- Vervoort, J.D., Patchett, P.J., Blichert-Toft, J., Albarède, F., 1999. Relationships between Lu–Hf and Sm–Nd isotopic systems in the global sedimentary system. *Earth Planet. Sci. Lett.* [https://doi.org/10.1016/S0012-821X\(99\)00047-3](https://doi.org/10.1016/S0012-821X(99)00047-3).
- Vorontsov, A.A., Yarmolyuk, V.V., Lykhin, D.A., Dril, S.I., Tatarnikov, S.A., Sandimirova, G.P., 2007. Magmatic sources and geodynamics of the early Mesozoic Northern Mongolia–Western Transbaikalia rift zone. *Petrol.* 15 (1), 35–57. <https://doi.org/10.1134/S0869591107010031>.
- Wang, Y., Foley, S.F., Buhre, S., Soldner, J., Xu, Y., 2021b. Origin of potassic postcollisional volcanic rocks in young, shallow, blueschist–rich lithosphere. *Sci. Adv.* 7 (29), eabc0291. <https://doi.org/10.1126/sciadv.abc0291>.
- Wang, T., Tong, Y., Zhang, L., Li, S., Huang, H., Zhang, J., Guo, L., Yang, Q., Hong, D., Donskaya, T., Gladkochub, D., Tserendash, N., 2017. Phanerozoic granitoids in the central and eastern parts of Central Asia and their tectonic significance. *J. Asian Earth Sci.* 145, 368–392. <https://doi.org/10.1016/j.jseae.2017.06.029>.
- Wang, T., Tong, Y., Xiao, W., Guo, L., Windley, B.F., Donskaya, T., Li, S., Tserendash, N., Zhang, J., 2021a. Rollback, scissor-like closure of the Mongol–Okhotsk Ocean and formation of an orocline: Magmatic migration based on a large archive of age data. *Nat. Sci. Rev.* nwab210. <https://doi.org/10.1093/nsr/nwab210>.
- Wang, Q., Wyman, D.A., Xu, J., Dong, Y., Vasconcelos, P.M., Pearson, N., Wan, Y., Dong, H., Li, C., Yu, Y., Zhu, T., Feng, X., Zhang, Q., Zi, F., Chu, Z., 2008. Eocene melting of subducting continental crust and early uplifting of central Tibet: Evidence from central–western Qiangtang high-K calc-alkaline andesites, dacites and rhyolites. *Earth Planet. Sci. Lett.* 272 (1–2), 158–171. <https://doi.org/10.1016/j.epsl.2008.04.034>.
- Wilhelm, C., Windley, B.F., Stampfli, G.M., 2012. The Altaids of Central Asia: A tectonic and evolutionary innovative review. *Earth Sci. Rev.* 113 (3–4), 303–341. <https://doi.org/10.1016/j.earscirev.2012.04.001>.
- Wilson, M., 1989. *Igneous petrogenesis*. Springer, Netherlands, Dordrecht.
- Windley, B.F., Alexeiev, D., Xiao, W., Kröner, A., Badarch, G., 2007. Tectonic models for accretion of the Central Asian Orogenic Belt. *J. Geol. Soc.* 164 (1), 31–47. <https://doi.org/10.1144/0016-76492006-022>.
- Woodhead, J.D., Hergt, J.M., Davidson, J.P., Eggins, S.M., 2001. Hafnium isotope evidence for ‘conservative’ element mobility during subduction zone processes. *Earth Planet. Sci. Lett.* 192 (3), 331–346. [https://doi.org/10.1016/S0012-821X\(01\)00453-8](https://doi.org/10.1016/S0012-821X(01)00453-8).
- Wu, L., Kravchinsky, V.A., Potter, D.K., 2017. Apparent polar wander paths of the major Chinese blocks since the Late Paleozoic: Toward restoring the amalgamation history of east Eurasia. *Earth Sci. Rev.* 171, 492–519. <https://doi.org/10.1016/j.earscirev.2017.06.016>.
- Wu, F., Sun, D., Li, H., Jahn, B., Wilde, S., 2002. A-type granites in northeastern China: Age and geochemical constraints on their petrogenesis. *Chem. Geol.* 187 (1–2), 143–173. [https://doi.org/10.1016/S0009-2541\(02\)00018-9](https://doi.org/10.1016/S0009-2541(02)00018-9).
- Wu, F.-Y., Sun, D.-Y., Ge, W.-C., Zhang, Y.-B., Grant, M.L., Wilde, S.A., Jahn, B.-M., 2011. Geochronology of the Phanerozoic granitoids in northeastern China. *J. Asian Earth Sci.* 41 (1), 1–30. <https://doi.org/10.1016/j.jseae.2010.11.014>.
- Xiao, W., Windley, B.F., Hao, J., Zhai, M., 2003. Accretion leading to collision and the Permian Solonker suture, Inner Mongolia, China: Termination of the central Asian orogenic belt: Solonker suturing in inner Mongolia. *Tectonics* 22 (6), n/a–n/a. <https://doi.org/10.1029/2002TC001484>.
- Xiao, W., Windley, B.F., Badarch, G., Sun, S., Li, J., Qin, K., Wang, Z., 2004. Palaeozoic accretionary and convergent tectonics of the southern Altaids: Implications for the growth of Central Asia. *J. Geol. Soc.* 161 (3), 339–342. <https://doi.org/10.1144/0016-764903-165>.
- Xiao, W., Huang, B., Han, C., Sun, S., Li, J., 2010. A review of the western part of the Altaids: A key to understanding the architecture of accretionary orogens. *Gondwana Res.* 18 (2), 253–273. <https://doi.org/10.1016/j.gr.2010.01.007>.
- Xiao, W., Windley, B.F., Sun, S., Li, J., Huang, B., Han, C., Yuan, C., Sun, M., Chen, H., 2015. A Tale of Amalgamation of Three Permio–Triassic Collage Systems in Central Asia: Oroclines, Sutures, and Terminal Accretion. *Annu. Rev. Earth Planet. Sci.* 43 (1), 477–507. <https://doi.org/10.1146/annurev-earth-060614-105254>.
- Xiao, W., Windley, B.F., Han, C., Liu, W., Wan, B., Zhang, J., Ao, S., Zhang, Z., Song, D., 2018. Late Paleozoic to early Triassic multiple roll-back and oroclinal bending of the Mongolia collage in Central Asia. *Earth Sci. Rev.* 186, 94–128. <https://doi.org/10.1016/j.earscirev.2017.09.020>.
- Yarmolyuk, V.V., Kovalenko, V.I., Sal'nikova, E.B., Budnikov, S.V., Kovach, V.P., Kotov, A.B., Ponomarchuk, V.A., 2002. Tectono–Magmatic Zoning, Magma Sources, and Geodynamics of the Early Mesozoic Mongolia–Transbaikalia Province. *Geotectonics* 36 (4), 19.
- Yarmolyuk, V.V., Kovalenko, V.I., Sal'nikova, E. B., Kovach, V. P., Kozlovsky, A. M., Kotov, A. B., & Lebedev, V. I., 2008. Geochronology of igneous rocks and formation of the Late Paleozoic south Mongolian active margin of the Siberian continent. *Stratigraphy and Geological Correlation* 16 (2), 162–181. <https://doi.org/10.1134/S0869593808020056>.
- Yarmolyuk, V.V., Kozlovsky, A.M., Sal'nikova, E. B., Kozakov, I. K., Kotov, A. B., Lebedev, V. I., & Eenjin, G., 2013. Age of the Khangai batholith and challenge of polychronic batholith formation in Central Asia. *Doklady Earth Sci.* 452 (2), 1001–1007. <https://doi.org/10.1134/S1028334X13100176>.
- Zamboni, D., Gazel, E., Ryan, J.G., Cannatelli, C., Lucchi, F., Atlas, Z.D., Trela, J., Mazza, S.E., De Vivo, B., 2016. Contrasting sediment melt and fluid signatures for magma components in the Aeolian Arc: Implications for numerical modeling of subduction systems: Melt/fluid signatures at the aeolian arc. *Geochim. Geophys. Geosyst.* 17 (6), 2034–2053. <https://doi.org/10.1002/2016GC006301>.
- Zhao, L., Guo, F., Fan, W., Huang, M., 2019. Roles of Subducted Pelagic and Terrigenous Sediments in Early Jurassic Mafic Magmatism in NE China: Constraints on the Architecture of Paleo–Pacific Subduction Zone. *J. Geophys. Res. Solid Earth* 124 (3), 2525–2550. <https://doi.org/10.1029/2018JB016487>.
- Zhao, P., Xu, B., Jahn, B., 2017. The Mongol–Okhotsk Ocean subduction-related Permian peraluminous granites in northeastern Mongolia: Constraints from zircon U–Pb ages, whole-rock elemental and Sr–Nd–Hf isotopic compositions. *J. Asian Earth Sci.* 144, 225–242. <https://doi.org/10.1016/j.jseae.2017.03.022>.
- Zheng, Y.-F., 2019. Subduction zone geochemistry. *Geosci. Front.* 10 (4), 1223–1254. <https://doi.org/10.1016/j.gsf.2019.02.003>.
- Zheng, Y., Chen, R., Xu, Z., Zhang, S., 2016. The transport of water in subduction zones. *Sci. China Earth Sci.* 59 (4), 651–682. <https://doi.org/10.1007/s11430-015-5258-4>.
- Zhou, J.-B., Wilde, S.A., 2013. The crustal accretion history and tectonic evolution of the NE China segment of the Central Asian Orogenic Belt. *Gondwana Res.* 23 (4), 1365–1377. <https://doi.org/10.1016/j.gr.2012.05.012>.
- Zhu, R.-Z., Lai, S.-C., Qin, J.-F., Zhao, S.-W., Santosh, M., 2019. Petrogenesis of high-K calc-alkaline granodiorite and its enclaves from the SE Lhasa block, Tibet (SW China): Implications for recycled subducted sediments. *GSA Bull.* 131 (7–8), 1224–1238. <https://doi.org/10.1130/B1841.1>.

- Zhu, M., Zhang, F., Miao, L., Baatar, M., Anaad, C., Yang, S., Li, X., 2016. Geochronology and geochemistry of the Triassic bimodal volcanic rocks and coeval A-type granites of the Olzit area, Middle Mongolia: Implications for the tectonic evolution of Mongol-Okhotsk Ocean. *J. Asian Earth Sci.* 122, 41–57. <https://doi.org/10.1016/j.jseaes.2016.03.001>.
- Zhu, M., Wakabayashi, J., Pastor-Galán, D., Zhang, F., Ganbat, A., Miao, L., Yang, S., Wang, Z., 2023. Large-scale Permo-Triassic back-arc extensions of the Mongol-Okhotsk Ocean. *GSA Bull.* <https://doi.org/10.1130/B36644.1>.
- Zonenshain, L.P., Kuzmin, M.I., Natapov, L.M., 1990. Mongol-Okhotsk foldbelt. A plate-tectonic synthesis. AGU, *Geodynamics Series*, In *Geology of the USSR*.
- Zorin, Y.A., 1999. Geodynamics of the western part of the Mongolia-Okhotsk collisional belt, Trans-Baikal region (Russia) and Mongolia. *Tectonophysics* 306 (1), 33–56. [https://doi.org/10.1016/S0040-1951\(99\)00042-6](https://doi.org/10.1016/S0040-1951(99)00042-6).